# Synthesis and Characterization of End-Functionalized Cylindrical Polyelectrolyte Brushes from Poly(styrene sulfonate)

**Karen Lienkamp, Lucie Noé, Marie-Hélène Breniaux, Ingo Lieberwirth, Franziska Groehn, and Gerhard Wegner***

*Max Planck Institute for Polymer Research, Ackermannweg 10, 55128 Mainz, Germany*

*Received November 7, 2006; Revised Manuscript Received January 30, 2007*

ABSTRACT: Cylindrical polyelectrolyte brushes from poly(styrenesulfonate) were synthesized by polymer analogous hydrolysis from the corresponding dodecyl and ethyl ester brushes. These brushes were characterized in solution (GPC−MALLS, static and dynamic light scattering, SANS, and $^1$H NMR), and on solid interfaces (AFM and TEM). It was shown that the cylindrical brushes may form extended aggregates in solution. The aggregation behavior and the size and shape of the aggregates depend on the side chain length and the degree of saponification. For samples with identical backbone and side chain length, but varying degrees of ester hydrolysis, marked differences in the aggregation behavior were observed. Cylindrical end-functionalized polyelectrolyte brushes from poly(styrenesulfonate) were synthesized by a combination of anionic polymerization yielding an end-functionalized ATRP macroinitiator with a positively charged head group, atom transfer radical polymerization, and polymer analogous hydrolysis. The brushes and their precursors were characterized in solution by MALDI−TOF MS, $^1$H NMR, GPC−MALLS, static and dynamic light scattering, and cryo-TEM. These brushes were found to form complexes with negatively charged latex particles. They may be discussed as models to mimic proteoglycan in the proteoglycan−hyaluronic acid complex.

## Introduction

Self-organizing systems are ubiquitous in nature, the double-helix of DNA and the folding of protein structures being common examples. Another important example of self-organization in the human organism is the formation of proteoglycan aggregates with hyaluronic acid (Figure 1).[1] These aggregates are found throughout all extracellular compartments. Because of their ability to absorb large amounts of water and form gels, these complexes form a tissue that can undergo reversible compression in articular cartilage, giving elasticity to blood vessels and contributing to the structural integrity of many tissues such as skin or brain.[2] The most abundant proteoglycan−hyaluronic acid aggregate found in nature is the aggrecan−hyaluronic acid aggregate. Aggrecan is a linear polypeptide chain carrying a large number of anionic polysaccharide side chains, thus forming an anionic polymer brush. The linker between aggrecan and hyaluronic acid is a positively charged, claw-shaped protein, which is covalently attached to the aggrecan molecule.[1,3] Hyaluronic acid (hyaluronan) is a glycosaminoglycan consisting of a disaccharide repeat unit (D-glucuronic acid and *N*-acetylglucosamine with a molar mass of approximately $10^6-10^7$ g mol$^{-1}$. Because of its polyanionic nature, it is a linear rod-like molecule of 2−25 $\mu$m length.[4] Besides being a structural component of connective tissues, it forms loose hydrated matrices that enable cell division and migration, as well as adhesion of immune cells, and it plays a role in intracellular signaling.[2] The importance of hyaluronan in these processes is due to the ability of many proteins to bind to it. One such protein is contained in proteoglycans. These are anionic polymer brushes consisting of a core protein, to which heteropolysaccharide side chains are attached. They are produced in the cell by the Golgi apparatus by glycosilation of the core protein: first, a tetrasaccharide is attached, then glycosyl transferases add one sugar molecule after the other (which is much like a "grafting-from" reaction), followed by sulfonation of the sugar side chains.[3] The side chains of aggrecan, (the proteoglycan found in human cartilage), consist of chondroitin sulfate and keratane sulfate. A typical aggrecan brush consists of 150 side chains, each having a molar mass of 20 000 g mol$^{-1}$,[1] making a total of $3 \times 10^6$ g mol$^{-1}$ for the whole molecule. In living organisms, aggrecan and hyaluronic acid are synthesized and separately released into the extracellular compartment, where the aggrecan molecules bind to the hyaluronic acid molecule. The aggregates are nondissociating and nondisplaceable under physiological conditions.[5] The binding between the link protein and hyaluronan is mainly due to the formation of ionic bonds between about eight basic amino acids in the protein and the carboxylic acid groups of hyaluronan.[6] Besides the ionic component of the binding, there is evidence that hydrogen bonding and van der Waals forces also play a role.[7]

In order to understand the unusual mechanical properties of these aggregates, which act as biological lubricants, and to mimic them in synthetic products, the aim of this work was to produce model compounds for the proteoglycan−hyaluronic acid complex (Figure 1). As a model for the proteoglycan, end-functionalized poly(styrenesulfonate) (PSS) polyelectrolyte brushes with a positively charged linker were synthesized and characterized. In an attempt to model the proteoglycan−hyaluronic acid aggregates, the complexation behavior of these end-functionalized brushes toward negatively charged species was investigated. The structure of the materials was analyzed by imaging methods (cryo-TEM) and scattering techniques (static and dynamic light scattering).

Before attempting to synthesize such a complicated polymeric species, we had to review the existing methods to synthesize cylindrical polymer brushes ("bottle brushes"). These consist of a linear main-chain and polymeric side chains. Because of the highly branched architecture of these materials, their bulk and solution properties are exceedingly different from those of their linear analogues of comparable molecular weight: the

* Corresponding author. Fax: +49 6131 379 100. E-mail: wegner@mpip-mainz.mpg.de.

10.1021/ma062569b CCC: $37.00 
Published on Web 03/09/2007

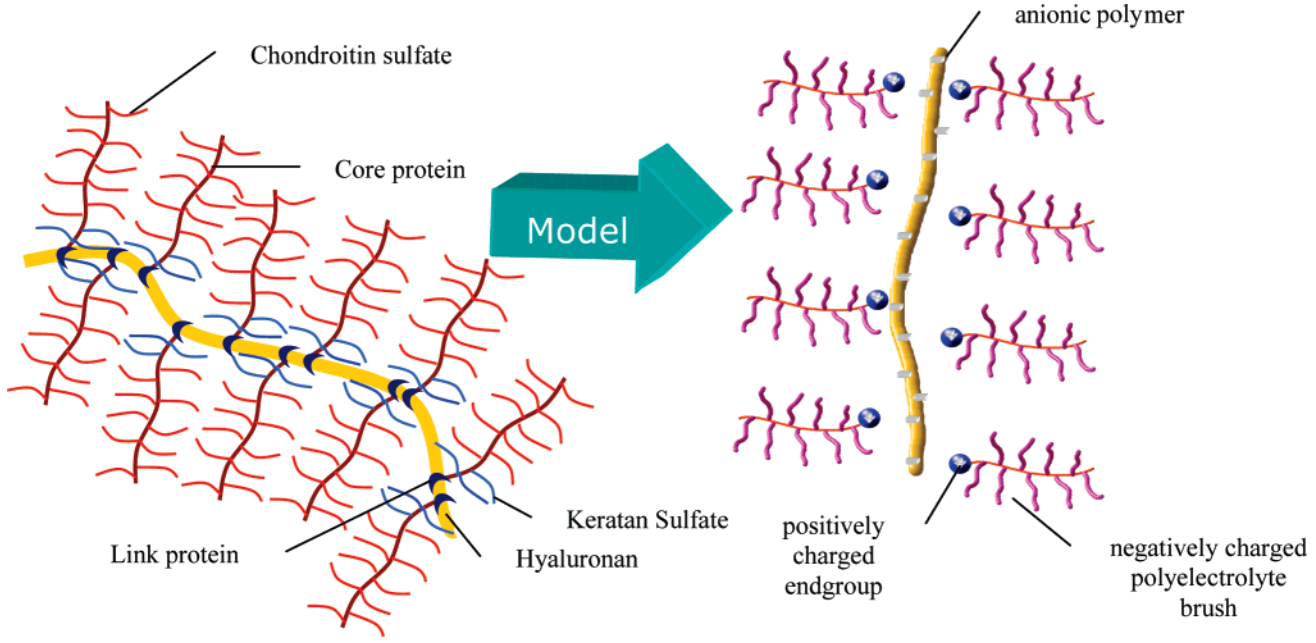


**Figure 1.** Cartoon representation of the proteoglycan−hyaluronic acid aggregates in human cartilage (left) and a simplified synthetic model system for this structure (right).

hydrodynamic radii are smaller, and the solution conformation depends on the length ratio of the side chains and the backbone.[8−11] The backbone being an "entropic spring" that strives for a coiled shape, the excluded volume interaction of the side chains lead to a more or less stretched molecular geometry.[12] It was confirmed by SAXS,[13] AFM,[14] and rheology[15] that polymer brushes do not entangle in bulk. Synthetic approaches toward polymer brushes are "grafting onto" ,[16−19] "grafting from" ,[20−25] and "grafting through" .[26−31]

Cylindrical PSS brushes thus far reported in the literature were obtained by sulfonation of poly(styrene) (PS) brushes: Schmidt et al.[32] obtained PSS brushes by sulfonation of PS poly(macromonomers). Only very recently, Fernyhough et al.[33−35] described the sulfonation of PS comb polymers obtained by "grafting onto" . However, polymer analogous sulfonation is never quantitative and often leads to structural imperfection (cross-linking and degradation) due to the harsh reaction conditions, which was also reported by Fernyhough et al. (increased polydispersity after sulfonation). We therefore synthesized cylindrical PSS brushes by hydrolysis of the corresponding esters,[36] as described below. The advantage of this method is that the complications of polymer-analogous sulfonation, i.e., incomplete and random sulfonation, cross-linking and degradation are avoided. The first part of this paper is dedicated to the synthesis of these structures, as depicted in Scheme 1. The structure of the materials was investigated by imaging methods (TEM, AFM) and scattering techniques (static and dynamic light scattering, SANS). The second part of the paper covers the end-functionalization (Scheme 2).

We would like to point out that the term "polyelectrolyte brush" is used rather indiscriminately in the literature for 1D-, 2D- and 3D-brushes [see ref 36]. The correct term for the type of molecule discussed in this paper is "cylindrical brush" , while "brush" usually refers to 2D- or 3D-brushes made up of chains attached to a 2D surface or a 3D object.

In a previous paper, polymerization of styrenesulfonate ethyl and dodecyl ester via ATRP ("grafting from" ) to obtain cylindrical polymer brushes was described.[36] The PSS brushes discussed in this paper were derived from these materials. For the reader's convenience, the molecular parameters determined for these samples are summarized in Table 1 (Sample Nomenclature: ***X*-*Y*-DZ** or ***X*-*Y*-E*Z***, ***X*** = brush backbone (**3** = 570 repeat units, **11** = 1600 repeat units), ***Y*** = grafting density, **D** = dodecyl ester, **E** = ethyl ester, ***Z*** = sample identification number)). Depending on the hydrolysis method used (a−d, see Scheme 1), the suffix, **a**−**d**, is added to the sample name of the hydrolyzed species to clarify the sample history. Unless otherwise stated, the free acid form is referred to.

## Experimental Part

**Synthesis.** All chemicals were bought from Aldrich, Fluka, or Acros and were used as received. Styrenesulfonate dodecyl ester was synthesized as described elsewhere.[37] Styrenesulfonate dodecyl ester brushes **1** (PSSD) and styrenesulfonate ethyl ester brushes **2** (PSSE) were synthesized as described elsewhere.[36] Poly(styrenesulfonate) brushes (**3a**−**3d**) were obtained via four hydrolysis procedures: (a) 100 mg (0.29 mmol SSD) of polymer was dissolved in a minimum amount of THF. Then 96 mg (2.9 mmol) of KOH (85%) was dissolved in Milli-Q $H_2O$ and added to this solution. The reaction mixture was kept at 60 °C for 3 days. It was then dialyzed vs 10 L Milli-Q water, which was exchanged every 24 h, until the conductivity of the water dropped to 0.1 $\mu$S after 12 h (membrane pore size 10 000 g/mol). Freeze-drying yielded the desired polyelectrolyte as the potassium salt. $^1$H NMR ($D_2O$, 80 °C): $\delta$ = 7.8−8.5 ($H_{meta}$), 7.5−6.7 ($H_{ortho}$), 4.3−5.5 ($H_{CH_2\ ester}$), 1.1−1.4 ($H_{CH_3\ ester}$) 1.4−1.9 ($H_{\beta-\omega\ CH_2\ ester}$), 0.9−3.0 ($H_{backbone}$). (b) First, 250 mg (0.71 mmol SSD) was dissolved in 20 mL of $CHCl_3$. Then 1 mL (7.10 mmol) of triethylamine was added. The reaction mixture was refluxed for 12 h and cooled to room temperature. The solvent was removed by vacuum evaporation. The reaction product was dissolved in 50 mL of Milli-Q $H_2O$. It was then dialyzed and freeze-dried as described above to obtain the PSS ammonium salt. $^1$H NMR ($D_2O$, 80 °C): $\delta$ = 7.8−8.5 ($H_{meta}$), 7.5−6.7 ($H_{ortho}$), 0.9−3.0 ($H_{backbone}$). (c) First, 250 mg (0.71 mmol SSD) were dissolved in 20 mL of $CHCl_3$. Then, 1 mL (7.10 mmol) of triethylamine was added. The reaction mixture was refluxed for 3 h and cooled to room temperature. The solvent was removed by vacuum evaporation. The reaction product was dissolved in 50 mL Milli-Q $H_2O$. Then, 240 mg (7.10 mmol) KOH (85%) was added. The reaction was refluxed for 48 h. It was then brought to pH = 1 with HCl and refluxed for 48 h. The solution was cooled to room temperature, dialyzed and freeze-dried as described above to yield the potassium salt. $^1$H NMR ($D_2O$, 80 °C): $\delta$ = 7.8−8.5 ($H_{meta}$),

**Scheme 1. Saponification of Polymer Brushes (1 for Dodecyl Ester and 2 for Ethyl Ester)**[a]

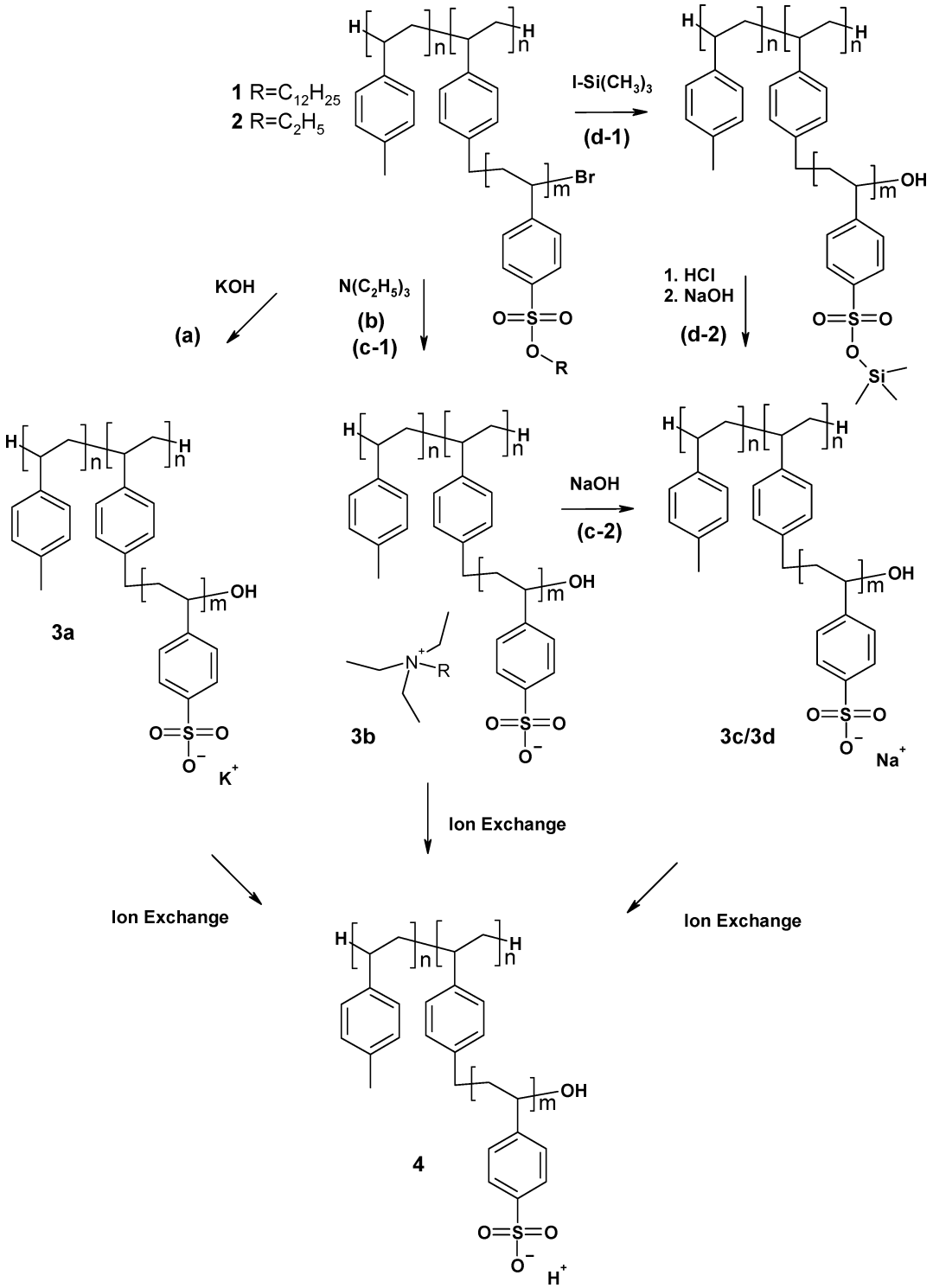


[a] Hydrolysis with KOH (a) yields polyelectrolyte brush **3a**; **3b** is obtained by saponification with $N(C_2H_5)_3$. This is also the first reaction step toward **3c** (c-1), which is followed by treatment with NaOH (c-2) to yield the product **3c**. **3d** is obtained by reaction with TMS−iodide (d-1) followed by hydrolysis with NaOH (d-2). In each case, the product is subject to ion exchange to yield **4**.

7.5−6.7 ($H_{ortho}$), 0.9−3.0 ($H_{backbone}$). (d) First, 150 mg (0.43 mmol SSD) was dissolved in 20 mL of $CH_2Cl_2$. Then, 856 mg (4.30 mmol) of trimethylsilyl iodide was added. The reaction mixture was refluxed for 12 h and cooled to room temperature. The solvent was removed by vacuum evaporation. The reaction product was dissolved in 50 mL of Milli-Q $H_2O$. Then 100 mL of 2 M NaOH was added. The reaction was stirred for 4 h. It was then dialyzed and freeze-dried to yield the sodium salt as described above. $^1H$ NMR ($D_2O$, 80 °C): $\delta$ = 7.8−8.5 ($H_{meta}$), 7.5−6.7 ($H_{ortho}$), 0.9−3.0 ($H_{backbone}$). PSSE brushes were hydrolyzed analogously: 50 mg (0.24 mmol SSE) was dissolved in 20 mLof $CH_2Cl_2$. Then 960 mg (2.40 mmol) of trimethylsilyl iodide was added. Following procedure d yielded the desired polyelectrolyte sodium salt. $^1H$ NMR ($D_2O$, 80 °C): $\delta$ = 7.8−8.5 ($H_{meta}$), 7.5−6.7 ($H_{ortho}$), 0.9−3.0 ($H_{backbone}$). Ion exchange to obtain **4**: 100 mg of the polyelectrolyte brush salt was dissolved in 100 mL of Milli-Q $H_2O$ and passed slowly (1 drop/min) over an ion-exchange resin (Amberlyte IR-120(+)). The solution was freeze-dried, redissolved in 50 mL of Milli-Q $H_2O$, and then dialyzed vs 10 L Milli-Q water, which was exchanged every 24 h, until the conductivity of the water dropped

**Scheme 2. Synthesis of End-Functionalized Polyelectrolyte Brushes**[a]

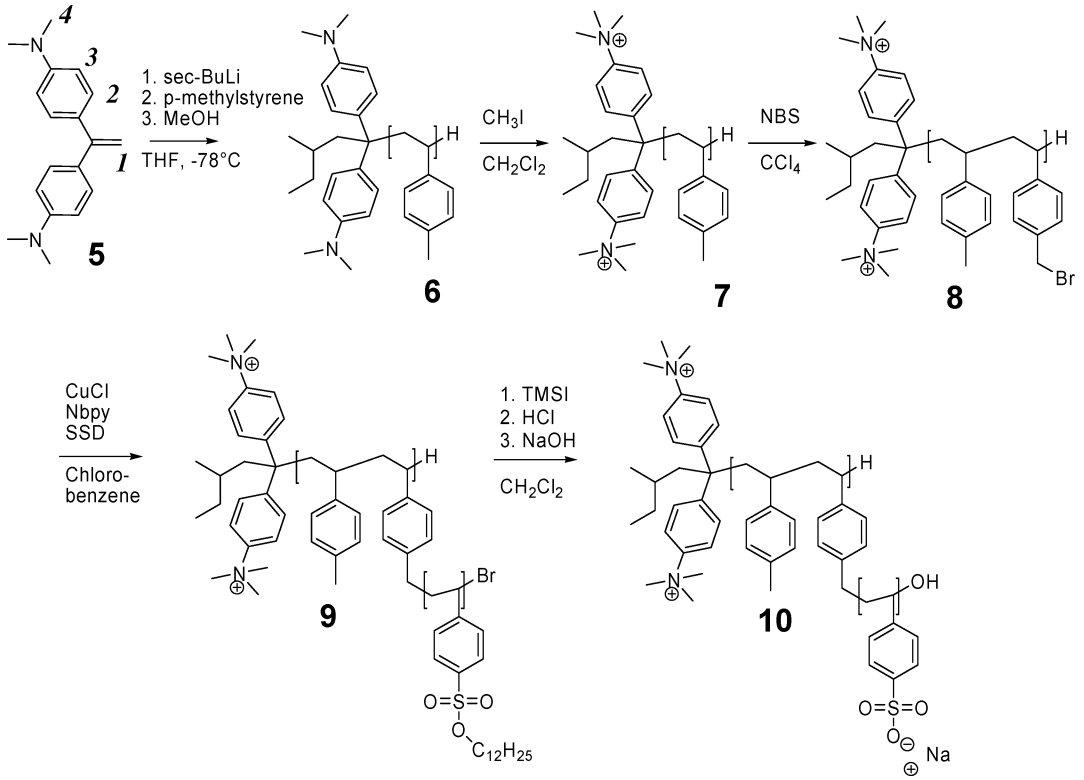


[a] After initiation of anionic polymerization with a functionalized initiator (**5**), the macroinitiator precursor 6 is obtained. Quarternization and bromination yields the macroinitiator **8**, from which the polymer brush **9** is obtained by ATRP. Saponification yields the end-functionalized polyelectrolyte brush **10**.

**Table 1. Molecular Parameters of the Parent Esters (Sample Nomenclature: *X-Y-DZ* or *X-Y-EZ*, *X* = Brush Backbone (3 = 570 Repeat Units, 11 = 1600 Repeat Units), *Y* = Grafting Density, D = Dodecyl Ester, E = Ethyl Ester, *Z* = Sample Identification Number)**[a]

| | GPC−MALLS | | | | | | $^1$H NMR | |
|---|---|---|---|---|---|---|---|---|
| sample | $M_w \times 10^{-3}$ [g/mol] | $M_n \times 10^{-3}$ [g/mol] | $M_w/M_n$ | $R_{g,z}$ [nm] | recovery rate | $n_{n,\ GPC-MALLS}$ | $n_{n,\ NMR}$ | $M_n \times 10^{-3}$ [g/mol] |
| **3-30-D1** | PSSD esters do not elute from column | 18 | 1008 | | | | | |
| **11-30-D2** | | | | | | | | |
| **11-20-E1** | 2739 | 2377 | 1.2 | 51 | 1.03 | 32 | 19 | 1388 |
| **11-40-E4** | 3256 | 1490 | 2.1 | 64 | 1.03 | 9 | 40 | 4848 |
| **11-60-E1** | 1577 | 702 | 2.3 | 61 | 0.87 | 3 | 24 | 4391 |

[a] Analytical data from GPC−MALLS (DMF, 0.1 M $NaNO_3$) and $^1$H NMR ($CD_2Cl_2$ for D samples, acetone-$d_6$ for E samples)

to 0.1 $\mu$S after 12 h (membrane pore size 10 000 g/mol). Freeze-drying yielded the desired poly(styrene sulfonic acid) brushes.

The functionalized initiator **5** was synthesized as described by Wittig[38] and Quirk:[39] 8.36 g (20.6 mmol) of triphenylphosphonium iodide was dissolved in 100 mL of dry diethyl ether under argon atmosphere. Then 16.1 mL (20.6 mmol) of methyl lithium was slowly added at room temperature. After an intense gas development, a colorless precipitate of lithium iodide appeared. The solution was stirred for 4 h and then filtered with a reverse frit under argon. The yellow solution was cooled to 0 °C. A 5.00 g (18.7 mmol) sample of 4,4′-bis(dimetylamino)benzophenone was suspended in 100 mL of dry THF under argon atmosphere. The blue suspension was added slowly to the cooled ylid solution with a steel transfer needle. The reaction mixture was allowed to warm to room temperature over night. In was then quenched with 30 mL of methanol and 10 mL of water. After cessation of the gas development, the solution was filtered. The solvent was removed by vacuum evaporation. The remaining solid was three times recrystallized from methanol and dried in vacuum. A white solid was obtained. $^1$H NMR ($CDCl_3$): $\delta$ = 7.25 (d, 4H, $H^2$), 6.65 (d, 4H, $H^3$), 5.15 (s, 2H, $H^1$), 2.90 (s, 12 H, $H^4$); MS (70 eV): 266.6 ($M^+$), 267.6 ($M + H^+$), 268.5 ($M + 2H^+$), 530.9 (dimer); Anal. Calcd for $C_{16}H_{19}N_2$ (239.34): C, 81.16; H, 8.32; N, 10.52. Found: C, 81.05; H, 8.36; N, 10.55. Synthesis of end-functionalized poly(*p*-methylstyrene) **2**: Following standard procedures for anionic polymerization, *p*-methylstyrene was and purified by high-vacuum distillation from fluorenyl-lithium. THF (200 mL) was distilled into the reactor. 0.4 mL ($c$ = 0.13 mol/L, 0.05 mmol) *sec*-butyl lithium were added to 133 mg (0.5 mmol) 1,1-di(4-dimethylaminophenyl)-ethylene) (**5**). At −78 °C, *p*-methylstyrene was added to the deep red solution. The reaction completed in 3 h. Precipitation into methanol yielded **6**. $^1$H NMR ($CD_2Cl_2$): $\delta$ = 6.6−6.7 ($H_{arom}$), 6.1−6.5 ($H_{arom}$), 1.9−2.2 ($H_{CH_3}$), 0.9−1.9 ($H_{backbone}$). Anal. Calcd for $C_{22}H_{32}N_2(C_9H_{10})_n$ (324.51 + (118.18)$_n$): C, 91.45; H, 8.53; N, 0.01. Found: C, 91.47; H, 8.64; N, <0.1. The quarternized species **7** was synthesized by dissolving 500 mg (4.23 mmol) of poly(*p*-methylstyrene) **6** in 50 mL of dry $CH_2Cl_2$ under argon; 6.00 g (42.3 mmol) methyl iodide was added. The reaction was stirred for 4 h at room temperature. The solvent was evaporated. Precipitation into methanol yielded **7**. $^1$H NMR ($CD_2Cl_2$): $\delta$ = 6.6−7.1 ($H_{arom}$), 6.1−6.6 ($H_{arom}$), 2.0−2.3 ($H_{CH3}$), 1.0−1.8 ($H_{backbone}$). Anal. Calcd for $C_{24}H_{38}N_2(C_9H_{10})_n$ (354.58 + (118.18)$_n$): C, 91.45; H, 8.53; N, 0.01. Found: C, 91.49; H, 8.52; N, <0.1. The macroinitiator **8** was obtained by dissolving 200 mg (1.69 mmol) **7** in 100 mL of dry $CCl_4$ under argon; 83.8 mg (0.846 mmol, 50 mol %) of dry *N*-bromosuccinimide (NBS) and 0.03 mol % of azoisobutyricacid nitrile (AIBN) were added. After refluxing 4 h, succinimid was removed by filtration. The solvent was evaporated. Precipitation into methanol yielded **8**. $^1$H NMR ($CD_2Cl_2$): $\delta$ = 6.6−7.0 ($H_{arom}$), 6.1−6.5 ($H_{arom}$), 4.2−4.4 ($H_{CH_2-Br}$), 2.0−2.3 ($H_{CH_3}$), 1.0−1.9

**Table 2. Characterization of Polyelectrolyte Brush Solutions**[a]

(a) GPC−MALLS Results

| sample | parent ester | d*n*/d*c* | $M_{w,\ MALLS} \times 10^{-6}$ [g/mol] | $M_w/M_n$ | % hydrolysis | $n_{n,\ sidechain}$ |
|---|---|---|---|---|---|---|
| **3-30-1a** | **3-30-D1** | 0.160 | 1.59 | 1.25 | 10 | |
| **3-30-1b** | **3-30-D1** | 0.160 | 0.71 | 1.46 | 40 | |
| **3-30-1c** | **3-30-D1** | 0.160 | 0.92 | 1.30 | 90 | |
| **3-30-1d** | **3-30-D1** | 0.160 | 0.85 | 1.48 | 66 | 16 |
| **11-30-2d** | **11-30-D2** | 0.161 | 1.61 | 1.17 | 66 | 12.8 |
| **11-40-IVd** | **11-40-E4** | 0.170 | 1.37 | 1.45 | 66 | 4.1 |
| **11-60-Id** | **11-60-E1** | 0.170 | 1.52 | | 66 | 5.4 |
| **11-20-Id ($Na^+$)** | **11-20-E1** | 0.167 | 2.07 | 1.78 | 66 | 13.3 |
| **11-40-IVd ($Na^+$)** | **11-40-E4** | 0.167 | 1.74 | 1.38 | 66 | 6.7 |
| **11-60-Id ($Na^+$)** | **11-60-E1** | 0.167 | 1.56 | 1.20 | 66 | 5.0 |

(b) Static and Dynamic Light Scattering Results

| sample | $M_{w,\ SLS} \times 10^{-6}$ [g/mol] | $A_2$ [mol L/g$^2$] | $R_g$ [nm] | $R_h$ [nm] | $\rho$ | $N_{agg}$ |
|---|---|---|---|---|---|---|
| **3-30-1a** | 142 | $2 \times 10^{-7}$ | 154 | 106 | 1.45 | 97 |
| **3-30-1b** | 21.7 | $4 \times 10^{-10}$ | 54.3 | 70.4 | 0.771 | 31 |
| **3-30-1d** | 1.60 | $1 \times 10^{-7}$ | 49.1 | 59.1 | 0.760 | 1.9 |
| **11-30-2d** | 2.60 | $6 \times 10^{-7}$ | 64.3 | 28.3 | 2.27 | 1.6 |
| **11-40-IVd** | 14.1 | $-2 \times 10^{-7}$ | 58.3 | 76.2 | 0.765 | 10 |
| **11-40-IVd ($Na^+$)** | 13.3 | $1 \times 10^{-8}$ | 62.8 | 83.9 | 0.778 | 7.8 |
| **11-60-Id** | 1.60 | $2 \times 10^{-7}$ | 61.8 | 48.3 | 1.28 | 1.1 |
| **11-60-Id ($Na^+$)** | 2.51 | $6 \times 10^{-7}$ | 67.6 | 37.8 | 1.79 | 1.6 |

[a] Key: (a) GPC−MALLS results (measured on MCX columns in $H_2O$/0.1 mol $L^{-1}$ $NaNO_3$) and degree of hydrolysis (by acid−base titration with $1 \times 10^{-3}$ mol $L^{-1}$ NaOH); (b) static and dynamic light scattering results. Measurements were performed in $H_2O$ with 1 mol $L^{-1}$ LiBr; the last letters in the sample name indicate the method of saponification: (a) KOH; (b) $N(CH_2H_5)_3$; (c) (1) $N(CH_2H_5)_3$, (2) KOH; (d) (1) TMS−I, (2) NaOH. Side chain lengths were calculated as follows: $n_n = (M_{n,brush} - M_{n,initiator})/(number\ of\ initiating\ sites\ per\ initiator\ molecule \times molecular\ mass\ of\ the\ repeat\ unit)$; parameters for macroinitiators taken from ref 36. $M_{n,brush}$ was calculated from $M_{w,brush}$ and the polydispersity (see text); i.e. the uncertainty in the polydispersity strongly affects also these values. The aggregation numbers were obtained by dividing $M_{w,\ SLS}$ by $M_{w,\ MALLS}$.

($H_{backbone}$). Anal. Calcd for $C_{24}H_{38}N_2(C_9H_{10})_n(C_9H_9Br)_m$ $(354.58 + (118.18)_n + (197.08)_m)$: C, 65.82; H, 5.99; Br, 26.19. Found: C, 65.30; H, 5.48; Br, 26.19. To synthesize the end-functionalized polymer brush **9**, 31.4 mg (0.318 mmol) of copper chloride and 260 mg (0.644 mmol) of 4,4′-dinonyl-2,2′-bipyridyl were subject to three freeze−thaw cycles and dissolved in 3.5 mL of oxygen-free chlorobenzene under argon in a Schlenk tube. Then 50 mg (0.318 mmol) of **8** was subject to three freeze−thaw cycles and dissolved in 3.5 mL of chlorobenzene under argon in a separate flask. A 5.00 g (14.2 mmol) sample of SSD was dissolved in acetone. The solvent was removed by evaporation. The solid monomer was molten at 40 °C under argon and added to the dark brown copper-ligand complex with a syringe. After 5 min of stirring, the macroinitiator solution was added. The Schlenk tube was placed into a preheated oil bath at 60 °C for 48 h. After cooling, the mixture was dissolved in 10 mL of THF and precipitated into 100 mL of methanol. After filtration and drying, the green solid was dissolved in THF. The remaining copper was removed ion exchange in acetone (Amberlyst 15, Fluka). The solution was precipitated into cold methanol. After filtration and drying, **9** was obtained as a colorless solid. $^1$H NMR ($CD_2Cl_2$): $\delta$ = 6.5−8.5 ($H_{arom}$), 4.0−4.5 ($H_{\alpha-CH_2}$), 1.9−2.2 ($H_{CH_3-styrene}$) 1.2−1.6 ($H_{\beta-\omega\ CH_2}$), 0.9−1.9 ($H_{backbone}$), 0.8−1.2 ($H_{CH_3-dodecylester}$). Anal. Calcd for $C_{24}H_{38}N_2(C_9H_{10})_n(C_9H_9Br(C_{20}H_{32}O_3S)_k)_m$ $(354.58 + (118.18)_n + (197.08 + (352.54)_k)_m)$: C, 68.11; H, 8.90; O, 12.53; S, 8.37; Br, 2.09. Found: C, 67.61; H, 9.23; O, 12.77; S, 8.90, 0.39. To obtain the end-functionalized polyelectrolyte brush **10**, 150 mg (0.43 mmol SSD) of **9** were dissolved in 100 mL of $CH_2Cl_2$. Then, 1.71 g (8.60 mmol) of trimethylsilyl iodide was added. The reaction mixture was refluxed for 4 h and cooled to room temperature. The solvent was evaporated. The reaction product was dissolved in 50 mL of Milli-Q $H_2O$ and freeze-dried. It was then redissolved in 100 mL 2 M NaOH. The reaction was stirred for 12 h and then dialyzed vs 10 L of Milli-Q water (membrane pore size 10 000 g/mol, water exchange every day). Freeze-drying yielded the desired polyelectrolyte sodium salt **10**. $^1$H NMR ($D_2O$, 80 °C): 20 °C): $\delta$ = 7.8−8.5 ($H_{aromPSS}$), 7.5−6.7 ($H_{aromPS}$), 0.9−3.0 ($H_{aliphPSS+PS}$).

**Light Scattering.** The static and dynamic light scattering measurements (SLS and DLS) were performed on a light scattering line with an ALV 5000 correlator (ALV, Langen), an ALV-SP81 goniometer, an avalanche photodiode and a krypton ion laser (647.1 nm). The samples were dissolved in Milli-Q water (Ultrapure Water purification unit, Millipore, Bedford) with a conductivity of 0.1 $\mu$S) and filtered with 0.2 $\mu$m Millex cellulose membrane filters (Millipore, Bedford) into dust free light scattering cells. SLS was measured from 30 to 150° in intervals of 5°; DLS was measured in intervals of 20°.

**Gel Permeation Chromatography (GPC) and GPC—MALLS.** GPC measuring units with a Waters-515 pump, Waters autosampler, column oven, column set (precolumn, two GPC columns; DMF, $T$ = 60−80 °C, Suprema column (PSS, Mainz); THF, room temperature, SDV column (PSS, Mainz); $H_2O$, $T$ = 60−80 °C, MCX column (PSS, Mainz); flow rate 0.5−1 mL/min, $c$ (Polymer) = 1 g $L^{-1}$, $c$ (salt) = 0.01−1 g $L^{-1}$; salt used, $NaNO_3$ or LiBr, as indicated), Soma S 3702 UV detector (GPC) or Wyatt Dawn Eos detector (MALLS), ERC RI-101 detector, and PSS GPC software were used. The samples were filtered with 0.45 $\mu$m Millex cellulose ester membrane filters (Millipore, Bedford) before injection.

**Measurement of the Refractive Index Increment.** The refractive index increment was measured on a Michelson scanning interferometer as described elsewhere.[40] The results are given in Table 2a.

**Elemental Analysis.** Elemental analyses were performed by Analytische Laboratorien Prof. Dr. H. Malissa and G. Reuter GmbH, Lindlar, Germany.

**Transmission Electron Microscopy (TEM).** Samples shaded with W/Ta (by electron beam evaporation of tungsten and tantalum on a Balzers evaporation equipment) were measured on a LEO EM 912 with 1K CCD camera. Cryo-TEM samples were prepared with a Vitrobot preparation unit on gold-coated holey carbon films and measured on a FEI Tecnai with 4K CCD camera.

**Atomic Force Microscopy (AFM).** All AFM images were measured on a NanoScope IIIa (Veeco Inc., Santa Barbara) using Nanoscope Software V. 5.12r. An E scanner with a scan size of 12 $\mu$m × 12 $\mu$m was used. All images were recorded in the tapping mode. Olympus OMCL-AC160TN-W2 cantilevers and DP 15 (MikroMasch, Talin) were used. Sample solutions ($10^{-7}$ to 1 g $L^{-1}$

in $H_2O$) were spin-coated on freshly cleaved mica surfaces (1000−2000 rpm, 60−120 s).

**MALDI—TOF Mass Spectrometry.** MALDI−TOF mass spectra were measured on a Bruker time-of-flight Reflex III mass spectrometer. The matrix used was dithranol.

**$^1$H NMR Measurements in Solution.** All $^1$H NMR solution spectra were measured on a Bruker 300 MHz Avance NMR spectrometer. The samples (1−100 mg) were dissolved in the specified deuterated solvent (0.6 mL) and put into NMR tubes with a 5 mm diameter. The samples were measured at room temperature unless otherwise specified.

**Small-Angle Neutron Scattering.** The dried samples were dissolved in $D_2O$, stirred, and heated to 80 °C for 2 h. After cooling to room temperature and stirring over night, the samples were filtered with 0.2 $\mu$m Millex cellulose membrane filters (Millipore, Bedford) into SANS cells and measured at the Paul-Scherrer-Institut, Villigen, Switzerland. Detector to sample distances of 2, 6, and 18 m were used.

## Results and Discussion

**1. Cylindrical Polyelectrolyte Brushes without End-Group. Synthesis.** To obtain quantitatively saponified PSS brushes (**4**), the dodecyl ester **1** and the ethyl ester **2** were subject to different hydrolysis conditions. As described by Woeste,[37] linear poly(styrenesulfonate esters) can be quantitatively hydrolyzed by potassium hydroxide, potassium acetate, barium hydroxide or ammonium carbonate. In the last case, the free acid form is available, in the other cases, the salt is obtained. More recent literature[41] suggests that linear poly(styrenesulfonate alkyl esters) can also be quantitatively saponified by a transesterification with trimethylsilyl iodide, followed by hydrolysis of the resulting silylether. Contrary to the linear esters, for the *cylindrical PSSD brushes* we found that quantitative hydrolysis is difficult and could not be obtained by either method. For the parent ester **3-30-D1**, four different hydrolysis conditions were tested (Scheme 1). Method a led to a phase separation of the mixture, followed by precipitation of the polyelectrolyte **3a**. After ion exchange, the degree of saponification of the product (**4**, sample **3-30-1a**; cf. Table 2a) was 10% (acid−base titration with 0.001 M NaOH). Method b, conducted in an organic solvent and exploiting the alkylating properties of styrenesulfonate esters yielded, after ion exchange, the product (**4**, sample **3-30-1b**, cf. Table 2a), which was 40% hydrolyzed. Method c, the sequential hydrolysis with triethylamine, sodium hydroxide and HCl, led to a polymer that was found to contain 90% acid groups. However, due to the severe reaction conditions applied, a large fraction of the product (**4**, sample **3-30-1c**, cf. Table 2a) was insoluble. (d) Transesterification of **1** with trimethylsilyl iodide in $CH_2Cl_2$, followed by saponification of the silylether **3d** with NaOH and ion exchange led to a product (**4**, sample **3-30-1d**, cf. Table 2a) with at least 66% saponified groups. The PSSE brushes (**2**) were also hydrolyzed by procedure d, yielding **4** after ion exchange. The silylether was completely soluble in $CH_2Cl_2$, but due to the mild reaction conditions, complete saponification could not be obtained. The product **4** is water-soluble and not cross-linked, as shown by aqueous GPC (Figure 2a). $^1$H NMR spectra of selected polyelectrolyte brushes are shown in Figure 3. As expected, the signals from the ester residues (at 3.8, 1.9, and 1.3 ppm) are decreased in sample **3-30-1b** as compared to sample **3-30-1a**, which is in accordance with the findings from acid−base titration. The same is found for samples **3-30-1d** and **3-30-1c**.

**GPC—MALLS Results.** Due to their amphiphilicity, it was difficult to find a column/eluent system for GPC which would elute the polyelectrolyte samples **4** without tailing effects due to enthalpic interactions. The best system found was $H_2O$/0.1 g $L^{-1}$ $NaNO_3$ on MCX columns (PSS, Mainz). When looking closely at the curve shapes (Figure 2, parts a and b), it was observed that most samples are asymmetrical and show a shoulder or tailing at the low molecular weight flank of the curve. This is due to the fact that the parent molecules were derived in a "grafting-from" process and not an anionic polymerization yielding a Lorentz-shaped curve, i.e., smaller molecular weights are also obtained by "grafting-from" . Similar curves were obtained both from GPC on the parent esters and from analytical ultracentrifugation (AUC) on the parent ester (cf. ref 36). As AUC is a sedimentation measurement and does not involve the same amount of shear on individual molecules as GPC, it appears that the asymmetry toward the low molecular weight flank is not due to chain cleavage. Chain cleavage however can be observed in the GPC curve of sample **11-20-1d** (peaks at high elution volumes). A GPC curve of sample **3-30-1c** is not included as this sample did not elute quantitatively from the GPC column due to cross-linking during hydrolysis.

After off-line determination of the refractive index increments (see Table 2a), the molecular weights $M_w$ could be determined for two series of samples by GPC−MALLS, as shown in Table 2a. For samples from the **3** series (number of repeat units of the brush backbone $n_{n,backbone} = 570$),[36] the $M_w$ values obtained (lines 1−4 in Table 2a) reflect the different degrees of saponification of each species, which is lowest for **3-30-1a** and of the same order of magnitude for **3-30-1d** and **3-30-1b**. For **3-30-1c**, $M_w$ is again slightly higher due to partial cross-linking in the sample. Because of the different degrees of hydrolysis for these samples and the resulting uncertainty about the mass of the repeat unit, it does not make much sense to calculate side chain lengths from this datum; the side chain length results were therefore omitted. The polydispersities obtained here must be treated with care. First, due to the different degrees of saponification of the samples derived from **3-30-D1** (lines 1−4 in Table 2a), the enthalpic interactions of these samples with the column material is different, leading to a different tailing behavior and thus to different polydispersities. Second, for samples with the same degree of hydrolysis derived from different parent molecules, also marked differences in polydispersity were observed. This is due to a combination of several factors: (1) the parent molecules were obtained by "grafting from" synthesis. Here, the polydispersity depends on the reaction control, which is in turn connected to the density of the reactive sites on the macroinitiator and the backbone length; (2) branched molecules always lead to unusual elution behavior where the GPC separation does not only occur by molecular weight, as demonstrated in an excellent work by Schmidt et al.[31] This effect has not yet be fully explained, however it is an indication that the polydispersities obtained are not necessarily related to the actual molecular weight distribution of the sample.

The side chain length values were calculated as follows: $n = [M_n(\text{brush}) - M_n\ (\text{Macroinitiator})]/(\text{initiating sites per molecule} \times \text{molecular mass of the repeat unit})$.[36] The results obtained are self-consistent, as good agreement is found for **11-60-Id** and **11-40-IVd** with their corresponding sodium salts. The deviation from the side chain lengths of the parent esters **2** (Scheme 1, Table 1) determined by GPC−MALLS (**11-60-E1**, $n = 3.2$, deviation 36%; **11-40-E1**, $n = 9.9$, deviation 38%)[36] is reasonable for the cumulative experimental error of two d*n*/d*c* measurements and two GPC−MALLS measurements in different solvents. The side chain lengths calculated are minimum values as 100% initiation efficiency of the macroinitiator was assumed for their calculation.[36] A side chain length determination by $^1$H NMR was not attempted for the polyelec-

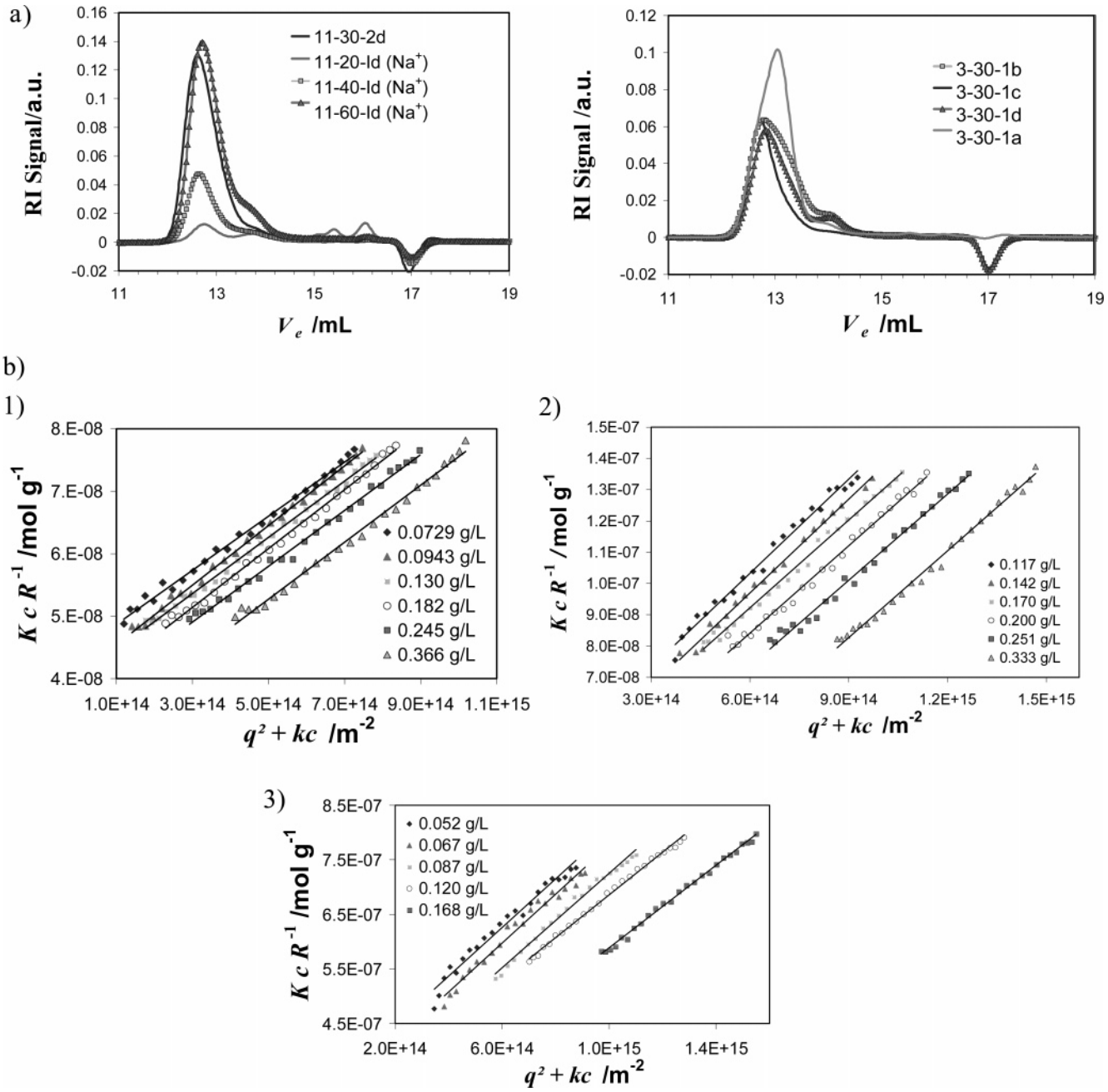


**Figure 2.** Characterization of polyelectrolyte brushes. (a) GPC−MALLS elugrams of polyelectrolyte brushes **4**: (1) **11** series; (2) **3** series. Measurements were performed on MCX columns ($H_2O$, 0.1 g $L^{-1}$ $NaNO_3$). (b) Static light scattering results (Zimm plots) for selected samples: (1) **3-30-1b**; (2) **11-40-IVb**; (3) **11-30-2d**. Samples measured in $H_2O$, 1 g $L^{-1}$ LiBr (cf. Table 2b).

trolyte brushes due to the broadness of the peaks and poor contrast to the background even at elevated temperatures (Figure 3).

**Light Scattering Results.** Selected samples were analyzed by static and dynamic light scattering. The experiments have been performed in water with 1 g $L^{-1}$ lithium bromide to suppress polyelectrolyte effects. In spite of their common chemical structure (poly(*p*-methylstyrene) backbone and poly(styrenesulfonate) side chains), the solubility of the samples was different. For some samples, molecular disperse solutions could only be obtained in DMF but not in water, where large aggregates were formed. The results from the static light scattering measurements are presented in Figure 2b) as Zimm plots. The hydrodynamic radii were obtained by dynamic light scattering (CONTIN[42] fit to the field autocorrelation function, Figure 4). The results obtained by static and dynamic light scattering are summarized in Table 2b).

The d*n*/d*c* values were obtained from the samples measured in an aqueous solution containing 1 g $L^{-1}$ LiBr. As pointed out by Kratochvíl,[43] aqueous solutions containing a low molecular weight electrolyte to suppress the polyelectrolyte effect must be considered as mixed solvents. Thus, the refractive index increment must be measured for a solution which is in osmotic equilibrium with the mixed solvent. If this is not done, the values determined for $M$, $A_2$, and $R_g$ are apparent values only. For the free acid form of the polyelectrolyte brushes used in this work, the effect proved to be negligible; the refractive index increment for sample **11-60-Id** measured in $H_2O$ was 0.170 mL/g, and it was 0.175 mL/g for the same sample measured in water with 1 g $L^{-1}$ LiBr. The value for the dialyzed solution must be between the two extremes. The ratio of the two values squared is 0.95; i.e., the error is 5%. As the concentration determination of the dialyzed solution is difficult and prone to be erroneous by at least the same amount, the solutions were not dialyzed,

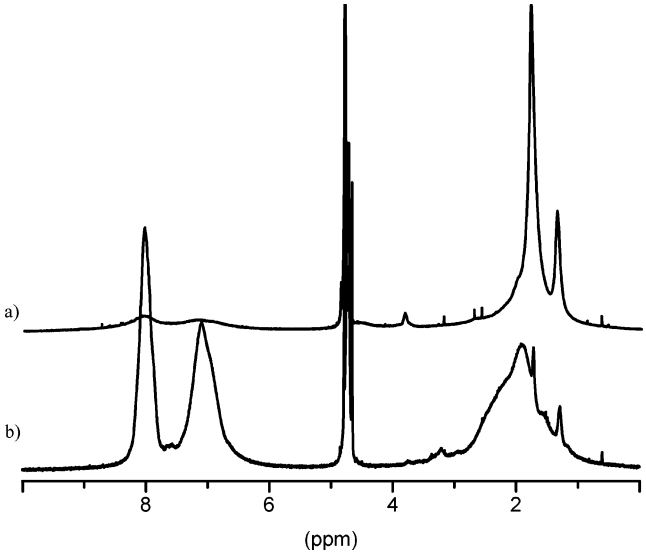


**Figure 3.** $^1$H NMR spectra of polyelectrolyte brushes in $D_2O$ : (a) **3-30-1a** and (b) **3-30-1b**. As can be seen from the intensity ratio of the aromatic peaks (6.5−9 ppm) to the aliphatic peaks (0.5−3 ppm), method b yields a higher degree of saponification than method a (cf. Table 2a).

but the refractive index increment values determined in 1 g $L^{-1}$ LiBr solutions were used.

The light scattering data obtained are difficult to interpret and due to the limited sample matrix not yet fully understood. Because of the complicated system involved, the light scattering data show a certain amount of data scattering; however the data were reproducible. From our as yet limited understanding of the system, we would like to highlight the following findings:

• The values obtained from static light scattering presented for $M_w$ in Table 2b are larger than those from GPC−MALLS (Table 2a). For samples **11-30-2d**, **11-60-Id**, **11-60-Id (Na$^+$)**, and **3-30-1d**, both values are on the same order of magnitude and the deviations may be attributed to the two different methods as the cumulative error of a MALLS, a light scattering and a d*n*/d*c* measurement. It is therefore concluded that, for these samples, monodisperse solutions were obtained and aggregation is negligible.

• For samples **11-40-IVd**, **11-40-IVd (Na$^+$)**, and the two other samples from the **3** series, the values differ considerably due to the formation of defined aggregates (see AFM and TEM images). By dividing the $M_w$ values from static light scattering by the $M_w$ values from GPC−MALLS, the number of molecules per aggregate $N_{agg}$ was estimated (see Table 2b). The values measured for the second virial coefficient $\boldsymbol{A}_2$ give a hint why such aggregates are only found for a few samples: for **11-40-IVd**, $A_2$ is by 2 orders of magnitude smaller than for the other samples, and for the corresponding sodium salt even negative. Thus, the contact with the bad solvent is avoided by intermolecular aggregation.

• Two samples from the **3** series also fit in this picture: For sample **3-30-1b**, also with a small $A_2$ value, large aggregates are found; sample **3-30-1d**, with a larger $A_2$ value ($1.40 \times 10^{-7}$ mol L $g^{-2}$), is molecularly disperse. The comparison between those two samples is particularly interesting as they differ only slightly in the degree of hydrolysis (40% for **3-30-1b** and 66% for **3-30-1d**). This shows the tremendous influence of the degree of hydrolysis for structure formation.

• Sample **3-30-1a**, with a low degree of hydrolysis (10%), forms again huge aggregates. Yet the $A_2$ value determined is on the same order of magnitude as for nonaggregating samples. As the values determined for the hydrodynamic radius and the radius of gyration are about 100 nm, it is possible that this structure is so large that it is already outside the range that is observable by light scattering methods, or the solution concentration is above the overlap concentration. Thus, the apparent values determined for $A_2$ and the other molecular parameters do not fit into the general picture.

• The $\rho = R_g/R_h$ values (cf. Table 2b), which are sensitive to the molecular shape as described in the literature,[44] indicate that the polyelectrolyte samples have different solution conformations. The aggregates of **11-40-IVd (Na$^+$)**, with longer side chains ($n = 10$ according to GPC−MALLS determined from the parent ester as described elsewhere[36]) and the corresponding free acid resemble to a homogeneous sphere ($\rho_{lit.}$[44] = 0.778). The conformation of the molecular disperse sample **11-30-2d** is that of a rigid rod ($\rho_{lit.}$[44] > 2.0). **11-60-Id**, with shorter side chains ($n = 3$ according to GPC−MALLS on the parent ester[36]) adopts a coil-like conformation. For the aggregates of sample **3-30-1b** and the single molecules of sample **3-30-1d**, a sphere-like geometry was found. This is interesting, as light scattering for sample **3-30-1d** was also measured in DMF. Here, a molecular weight $M_w$ of $7 \times 10^5$ g $mol^{-1}$ was found, with $R_g$ = 20.6 nm and $R_h$ = 11.6 nm, which gives a $\rho$ ratio of 1.78. As this value is in good accordance with the $M_w$ determined for this sample by GPC−MALLS in $H_2O$ ($M_w = 8.5 \times 10^5$ g $mol^{-1}$, it appears that the sample avoids the aqueous solvent by forming spheres, while it is molecular disperse in DMF and here also retains its wormlike geometry.

It should be mentioned that the $\rho$ parameter, while depending on the molecular shape, is also sensitive to the solvent quality and the broadness of the distribution. Both parameters increase the $\rho$ values.[46] These findings will be discussed with in combination with other results in the conclusion.

**SANS Results.** The cross-sectional radius of gyration $R_{g,c}$ was determined by small-angle neutron scattering. The SLS data are included in the plot of log $I$ vs log $q$ (Figure 5a). The $R_{g,c}$ values were determined from the initial slope of a plot of ln($Iq$) vs $q^2$. Sample **3-30-1a** (K$^+$), the potassium salt of **3-30-1a**, with only 10% hydrolysis, has the highest diameter due to the voluminous residual PSSD side chains; the samples with medium degrees of hydrolysis (**3-30-1b** and **3-30-1d**) have comparable and smaller radii, while $R_{g,c}$ of the almost fully saponified sample is smallest. This correlation between the cross-sectional radius of gyration and the degree of saponification is shown in Figure 5b. The cross-linked species and insoluble material were removed by filtration of the aqueous solution. As this changed the sample concentration tremendously, we did not use the data from SLS to determine $M_w$; however, it was good enough to use it as "calibration" to which the SANS curve could be shifted (this is the usual procedure when combining SLS and SANS data when the molecular structure of the sample is very complicated and thus the SANS data cannot be transferred into the same units as the SLS data). As the $q$ range from which the cross-section data was obtained does not "see" the whole molecule but only the cross-section, this datum can be used for the determination of $R_{g,c}$.

**Imaging.** Imaging of the polyelectrolyte brushes by AFM (tapping mode) was not as straight forward as in the case of the PSSD brushes,[36] as the polyelectrolyte brushes were not as firmly adsorbed on the mica surface as the corresponding esters. Also, due to the absence of the ester group, the mechanical contrast to the surface was worse. From the AFM images, it was concluded that the polyelectrolyte brushes are clustered into small groups, which is in accordance with the findings from

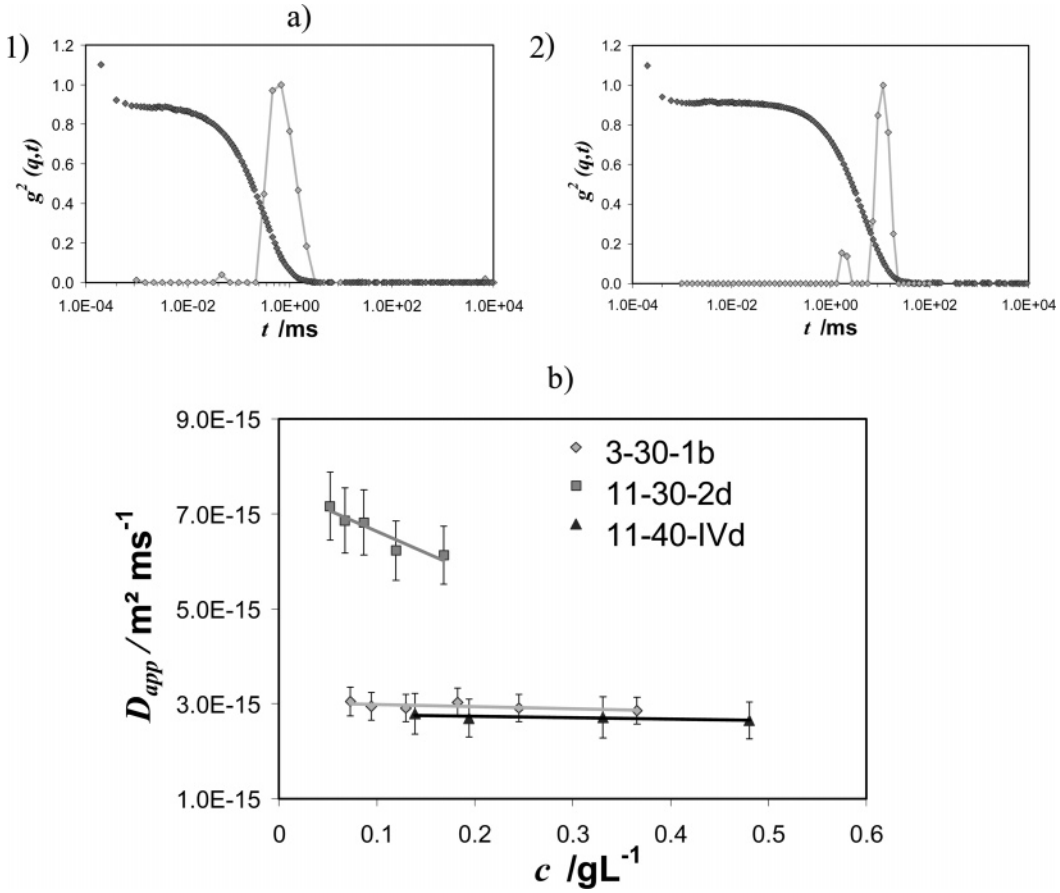


**Figure 4.** Characterization of the polyelectrolyte brushes. (a) Dynamic light scattering results (autocorrelation function and distribution of relaxation times) for selected samples: (1) **11-30-2d**; (2) **11-40-IVd**. (b) Determination of the diffusion coefficient for selected samples. All measurements in $H_2O$/1 mol $L^{-1}$ LiBr.

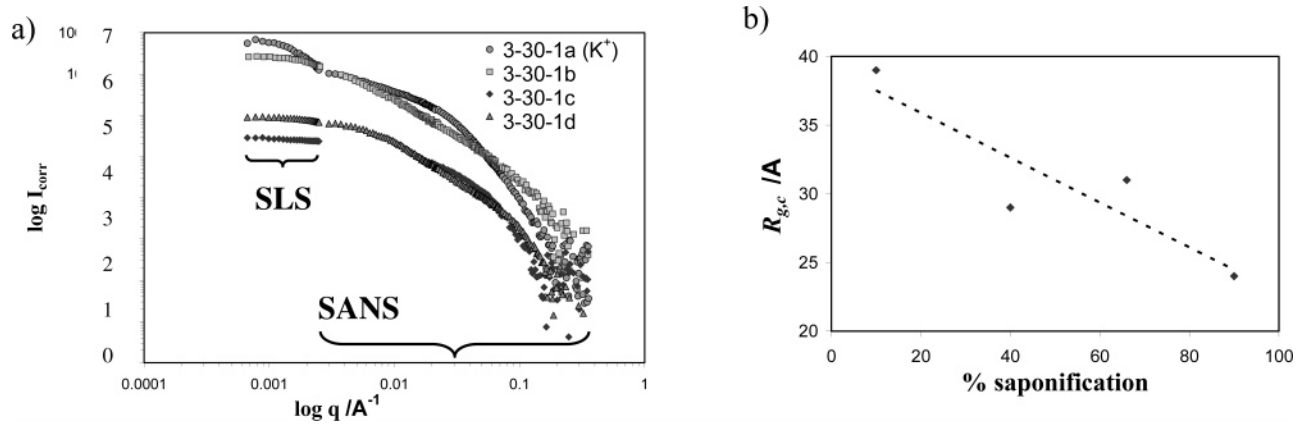


**Figure 5.** Characterization of polyelectrolyte brushes by small-angle neutron scattering: (a) log *I* vs log *q*, light scattering results (SLS) are included; (b) shows that there is a correlation of the degree of saponification to the radius of gyration for these samples.

static light scattering. It is therefore difficult to precisely determine the contour length and the molecule diameter. Table 3a gives best estimates for those values, as measured from the AFM images. The results indicate that the polyelectrolyte brushes derived from **3-30-D1** (contour length 78.5 nm, diameter 11.6 nm, height 1.04 nm)[36] are slightly shorter than the parent ester due to a contraction of the brush backbone in the absence of the large ester residues. Sample **3-30-1b ($NR_4^+$)** (which is the ammonium salt of **3-30-1b**, 3b in Scheme 1; cf. Figure 6a) is slightly longer and has a significantly larger diameter than the other polyelectrolyte brushes due to its large tetraalkylammonium counterions. Its diameter is larger than that of the parent ester, as the alkylammonium ions are more voluminous than the ester residue of **3-30-D1**. Moreover, they are not covalently connected to the molecule, i.e., the electrostatic attraction of the counterions is balanced by steric repulsion, making the whole molecule larger than the parent ester. In conclusion, the backbone of the polyelectrolyte brushes seems to be *more* coiled than that of the parent ester. It appears that side chains of the polyelectrolyte brushes **4** (chain length of $n_n = 18$)[36] are not voluminous enough to maintain the backbone stretching of the parent ester, leading to a contour length decrease of roughly 20%.

The aggregation of the polyelectrolyte brushes found by light scattering was also seen—at least in principle—by TEM and AFM. Figure 6b displays a TEM micrograph of sample **11-40-IVd ($Na^+$)** from the **11** series: long polymer strands with contour lengths of several micrometers are observed. The

**Table 3. Characterization of the Nonfunctionalized Polyelectrolyte Brushes**

(a) AFM Results[a]

| sample | contour length [nm] | diameter [nm] | height [nm] |
|---|---|---|---|
| **3-30-1a** | 51 ± 13 | 10 ± 2 | 1.1 ± 0.2 |
| **3-30-1b ($NR_4^+$)** | 66 ± 9 | 20 ± 3 | 1.6 ± 0.1 |
| **3-30-1d** | 56 ± 11 | 13 ± 3 | 1.1 ± 0.1 |
| **3-30-D1** | 79 ± 10 | 12 ± 2 | 1.1 ± 0.1 |

(b) TEM Results of Sample **11-40-IVd**[b]

| **11-40-IVd ($Na^+$)** | contour length [nm] | diameter [nm] |
|---|---|---|
| single molecules | 126 ± 11 | 15 ± 1 |
| single strand | | 13 ± 2 |
| double strand | several $\mu$m | 20 ± 2 |
| multiple strand | | 28 ± 3 |

[a] Samples spin coated on mica. [b] Spin coated on mica, shaded with W/Ta by electron beam evaporation.

diameters of these strands increase upon fusion of two strands at a junction. Table 3b summarizes the results obtained from TEM images. A cartoon representation of these structures is shown in the inset of Figure 6b. The single strands of the aggregates are slightly thinner than the single molecules. Because of the hydrophobicity of the polymer backbone and the hydrophilicity of the side chains, the following structure model is suggested: the polyelectrolyte backbones align parallel to each other on the carbon-coated mica surface. These backbones are surrounded by a corona of polyelectrolyte side chains. As a result of the backbone alignment the diameter of the double and eventually multiple strands is slightly smaller than twice or three times the diameter of the single strands, which supports the model proposed.

Aggregates of similar dimension, yet entirely different morphology, are found for **11-40-IVd** on mica (AFM, Tapping Mode): large defined aggregates with diameters of 59 ± 5 nm and 11 ± 1 nm height are observed (Figure 6c) are observed. SEM images (not shown) reveal that these structures are evenly distributed over the whole sample surface. Besides these aggregates, extended linear single molecules with a diameter of 11 ± 2 nm and 1.8 ± 0.5 nm height are observed in the phase image (stretched by fast spin-coating). Samples **11-40-IVd ($Na^+$)** and the corresponding free acid form, according to static light scattering, have the geometry of a homogeneous sphere in solution, whereas AFM and TEM reveal that these samples (on solid support) consists of large elongated aggregates. This apparent contradiction is rationalized as follows: the elongated aggregates wind up in solution to form a spherelike blob. The driving force of this transition could be minimization of solvent interactions.

The AFM images and TEM micrographs presented thus far gave the possibility to image single molecules on a solid substrate. The dimensions measured from such samples have only limited relation to the actual dimensions of the sample in solution due to deformation of the single molecule or aggregate on adhesion to the surface. Cryo-TEM is a useful alternative for imaging "as in solution". This is shown below for samples **11-60-Id** and **11-40-IVd**. Sample **11-60-Id** was stained by the addition of CsOH, which did not result in much contrast enhancement (Figure 7a). The brushes imaged had a diameter of 6.1 nm. Sample **11-40-IVd** (Figure 7b) was stained with CsCl and bovine serum albumin (BSA) as described for spherical polyelectrolyte brushes by Talmon and Ballauff.[46] BSA is a natural protein that has a good contrast in electron microscopy and was shown to migrate into polyelectrolyte brushes, thus making them visible in cryo-TEM. The image in Figure 7b shows a mesh-like structure that look like a superposition of the strand-like structure from sample **11-40-IVd ($Na^+$)** in Figure 6b. This makes sense as Figure 6b shows images obtained from a sample shaded with W/Ta, i.e., only the sample surface is visible. The cryo-TEM samples have a finite thickness, and the transmission image thus obtained is a projection of all elements in this area onto a 2D image or screen, i.e., the molecule strands with a highway junction-like shape put on top of each other will resemble a network-like entity. The diameter of the strands in image in Figure 7b is much smaller than expected (3.1 nm compared to the 13 nm single strands from Figure 6b). This could be another effect of the weak contrast, or the staining only affects the polymer backbone.

**Saponification.** As can be seen from the titration results (cf. Table 2a), quantitative hydrolysis of the polymer brushes could not be obtained. This is a contradiction to findings by Woeste[37] and others[47] on the saponification of linear PSSD and PSSE homopolymers. For those systems, quantitative hydrolysis was claimed. This discrepancy may be attributed to the more complicated polymer architecture of the brushes. On a qualitative basis, the following interpretation is suggested, taking into account the structural differences between linear and branched systems: As for any reaction, for quantitative hydrolysis, the free enthalpy of the overall reaction must be negative. Thus, entropic and enthalpic effects of the individual reaction steps need to be discussed. For the enthalpy parameter, the reaction enthalpy and the osmotic pressure of the polyelectrolyte brush need to be considered. The counterion condensation is certainly enhanced in the polyelectrolyte brush as compared to its linear analogue, as has been shown in the literature.[32] Due to the counterion condensation, the osmotic pressure in the brush is high, i.e., with increasing degree of saponification, it is increasingly difficult for any by its very nature ionogenic saponification agent to enter it. Also, the hydrophobic repulsion should be more pronounced in the case of the brush due to its branched architecture. These parameters make the reaction more unfavorable for the brush compared to the linear analogue. On the other hand, the gain of conformational and rotational entropy of the hydrolyzed ester residues is more pronounced in the case of the brush, as it has a much more confining environment than in a linear poly(styrenesulfonate ester). However, the experimental data show that this effect cannot compensate for the joint effect of the hydrophobic repulsion and the osmotic pressure, i.e., the degree of hydrolysis stays lower. For saponification method d, a strong enthalpic driving force of the reaction is the formation of a Si−O bond in the first reaction step, as well as the facilitated hydrolysis of the R′−OSi compared to R′−OR, $OTMS^-$ being a much better leaving group than the alcoholate. Thus, the conversion is higher than for methods a and b. The low conversion in reaction a is most probably due to the strong hydrophobic interactions. These also play a role in reaction d, yet due to the higher reaction enthalpy, this is compensated. The previous considerations lead to the following model for saponification: the saponification agent acts first in the molecule periphery, as this molecule part is more approachable than the ester groups near the core and the hydrophobic interactions are less pronounced. This decreases the hydrophobicity of the whole molecule. At the same time, the progressive saponification leads to an increased osmotic pressure due to counterion condensation. At a point depending on the specific reaction conditions (nature of the saponification agent, reaction enthalpy, temperature, etc.), the conversion of the hydrolysis in not increased further as the effect of the osmotic pressure does not allow the saponification

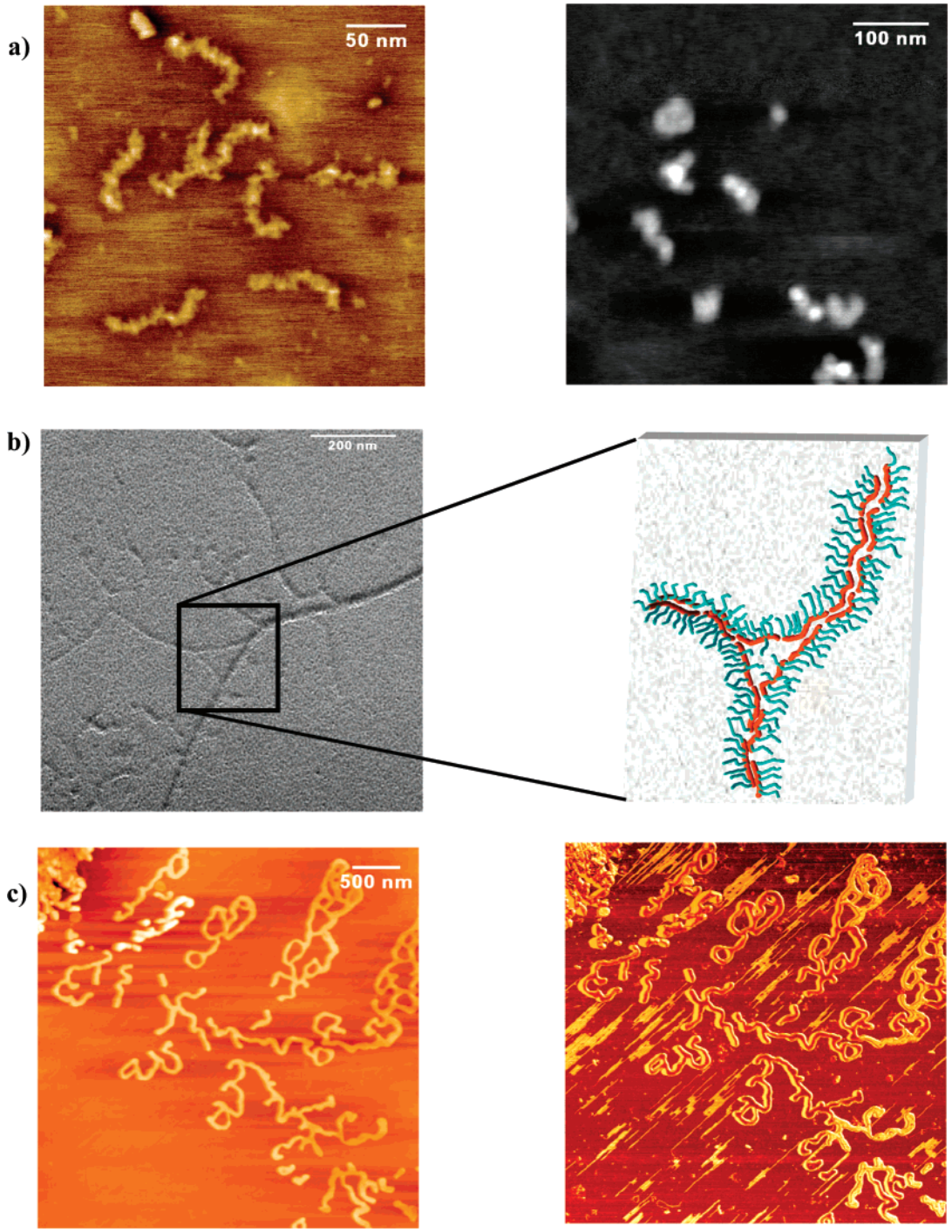


**Figure 6.** Imaging of polyelectrolyte brushes. (a) AFM height images of the parent ester (**3-30-D1**, left) and of single molecules of **3-30-1b** ($NR_4^+$) (right), both spin-coated on mica from THF and water, respectively, cf. Table 3. Because of the week absorption on the polyelectrolyte brushes on the substrate, the image is rather blurred as compared to the parent ester. (b) TEM image of aggregates of **11-40-IVd** ($Na^+$), spin-coated on carbon/mica from water, shaded with W/Ta. The illustration of part b shows a rationalization of the aggregate structure (cf. Table 3b). (c) AFM images (left, height; right, phase) of sample **11-40-IVd** spin-coated on mica from water.

agent to enter the molecule. As a result, we propose that the polyelectrolyte molecules described in this paper have an internal hydrophobicity gradient: it is hydrophobic inside near the backbone and hydrophilic in the periphery. The gradient assumption is supported by the following experimental findings: Polyelectrolyte brushes with different side chain lengths and different side chain-backbone length ratios show remarkable difference in their solution and aggregation behavior in water, as discussed above. Also, the polyelectrolyte brushes tend to align the backbones to form high molecular weight aggregates. The driving force of this aggregation is hydrophobic interaction, which are minimized by aligning the hydrophobic parts and exposing the hydrophilic parts to the surrounding water. This also explains why single molecules are found in DMF while aggregates are formed in water. In publications on poly(styrenesulfonate) comb polymers obtained by polymer analogous sulfonation (80%-100% sulfonation), no such aggregation was observed.[33−35] A more detailed discussion of this issue can be found elsewhere.[48]

**Proof of Concept.** The idea of cluster formation of the polyelectrolyte brushes due to hydrophobic interactions is further supported by the following experiment: 4-dimethylamino-2-

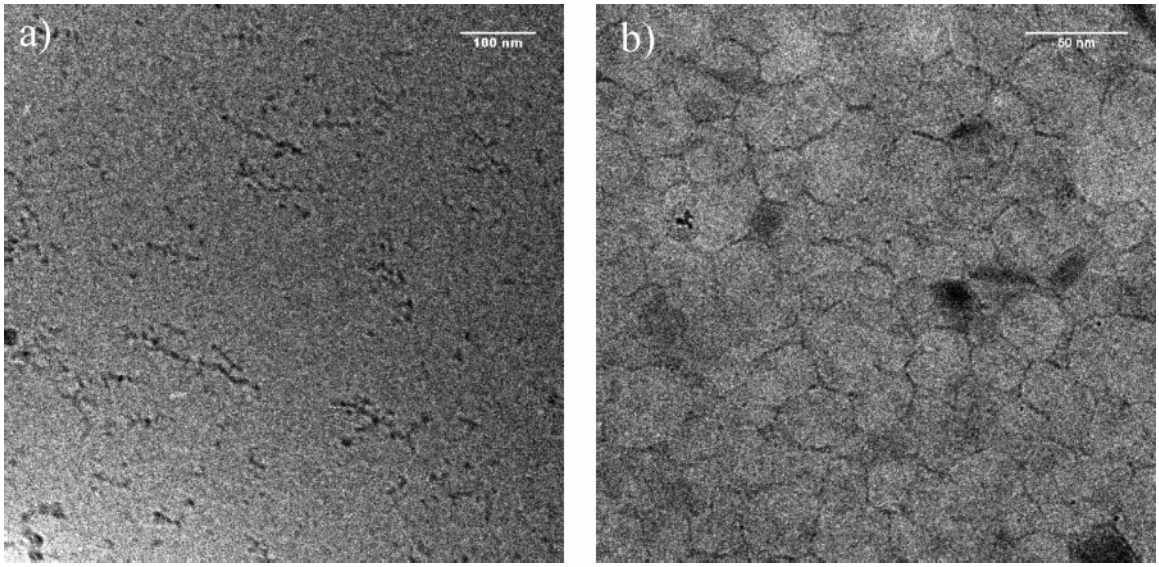


**Figure 7.** Cryo-TEM images of a) **11-60-Id** stained with $Cs^+$; (b) **11-40-IVd** stained with $Cs^+$ and BSA.

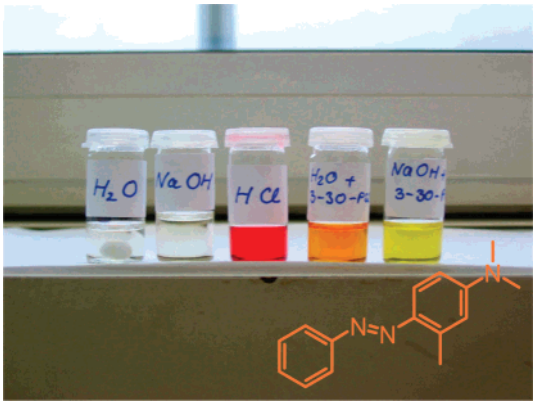


**Figure 8.** Solubilization of a hydrophobic azo dye (see inset) by polyelectrolyte brush **3-30-1a**; no solubilization occurs in pure $H_2O$ and NaOH (left). HCl causes solubilization by protonation (middle, red). Addition of **3-30-1a** to the NaOH solution results in a yellow solution (right), in which the dye is solubilized by the hydrophobic parts of the brush molecules. In aqueous solution, both solubilization mechanisms are present due to the brush's intrinsic acidity.

methylazobenzene (structure inset in Figure 8), which is insoluble in water and NaOH, but soluble in HCl due to protonation, is a classical dye for fat.[49] 1 mg of 4-dimethylamino-2-methylazobenzene have been added to 2 mL of $H_2O$, 2 mL of NaOH, 2 mL of HCl, 2 mL of $H_2O$ with 5 mg of **3-30-1a**, and 2 mL of NaOH with 5 mg **3-30-1a**. The results are shown in Figure 8. As expected, the dye is insoluble in water and NaOH. In HCl, it forms a pink-red solution due to protonation, causing a red shift of the dye absorption. In water with the polyelectrolyte brush, the solution is orange. To exclude the possibility that this solubilization is due to protonation of the primary amine of the dye, the experiment is repeated with NaOH and polyelectrolyte brush. Here, the solution is yellow, and the dye is completely dissolved. As the same amount of dye is used in all experiments, it can be concluded that the different colors are not due to concentration effects. In the case of the polymer in NaOH, the dye is solubilized within the hydrophobic part of the polyelectrolyte brush near the backbone, causing a yellow color. In $H_2O$ with polyelectrolyte, both mechanisms (protonation and solubilization by hydrophobic interactions) are active, which can be seen from the orange color. The comparison of the experiments with NaOH alone and NaOH with the polyelectrolyte proves that the polyelectrolyte addition causes the dye solubilization.

**Table 4. GPC−MALLS Results for the Functionalized Macroinitiator Precursors 6 and the Macroinitiators 7 (SDV, THF)**

| sample | $M_{n,theory} \times 10^{-3}$ [g/mol] | $M_{w,GPC-MALLS} \times 10^{-3}$ [g/mol] | $M_{n,GPC-MALLS} \times 10^{-3}$ [g/mol] | $M_w/M_n$ |
|---|---|---|---|---|
| **6b** | 200 | 212 | 196 | 1.10 |
| **7b** | 200 | 209 | 195 | 1.10 |
| **6a** | 7 | 8.2 | 7.9 | 1.04 |
| **7a** | 7 | 9.2 | 8.7 | 1.05 |

**2. End-Functionalized Cylindrical Polyelectrolyte Brushes.** Functionalized polymers with one head group can be obtained by different synthetic strategies. The most common ones are end-capping of a living polymer with a reagent carrying a functional group or initiation of a living polymerization with an initiator carrying a functional group. The synthetic procedure applied for the synthesis of ammonium end-functionalized polyelectrolyte brushes is shown in Scheme 2. Using *sec*-butyl lithium with an excess of **5** yielded an active initiator for methylstyrene polymerization. Applying standard procedures for the anionic polymerization of styrenic monomers, the functionalized macroinitiator precursor **6** was obtained. For the synthesis of proteoglycan models, high molecular weight was aimed at **(6b)**; however to be able to demonstrate the success of the functionalization, a low molecular weight model compound was also synthesized (**6a**). The analytical results of both compounds, as well as their quarternized analogues **7** are summarized in Table 4. Figure 9a shows the GPC elugram of **6b** and **7b**. The molar mass distribution of sample **6b** was reasonably narrow to use it as a macroinitiator precursor. The success of the functionalization was demonstrated with model compounds **6a** and **7a** by MALDI−TOF mass spectrometry. To avoid interpretation difficulties, the compounds were measured without salt added, although this naturally leads to a loss in the spectrum quality. The spectra are shown in Figure 9b. A comparison between the spectra clearly demonstrates that the desired functionalized polymer was obtained. A relative shift of 15 amu between the mass spectrum of **7a** compared to the nonquarternized compound **6a** was found, matching with the molecular weight of an additional methyl group. The fact that the spectrum is shifted by 15 amu and not 30 amu (two nitrogen atoms are quarternized) is due to plotting *m*/*z*. As $z = 2$ in this case ($M +$

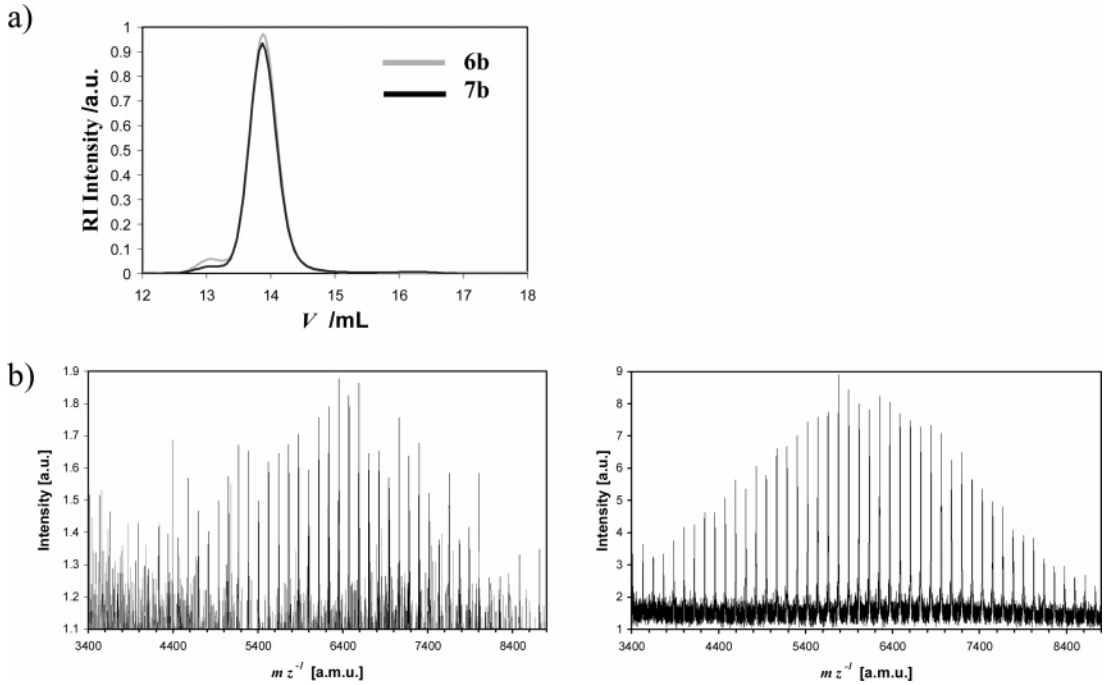


**Figure 9.** Characterization of the functionalized polyelectrolyte brushes: (a) GPC elugram of samples **6b** and **7b**, indicating that a low polydispersity was obtained with the functionalized initiator; (b) MALDI−TOF mass spectra of macroinitiator precursor **6a** (left) and macroinitiator precursor **7a** (right). The success of the quarternization can be seen from the increase of the signal intensity for the quarternized species **6a** and the relative peak shift as compared to **7a**.

30)/2 = $M' + 15$. Besides this characteristic shift, the spectrum intensity, which went up by a factor of 10 as compared to the nonquarternized spectrum (using identical sample preparation conditions), is a further indication of successful quarternization. The $^1$H NMR resonances of the head group are covered by the signals from the polymer and could not even be resolved on the 700 MHz spectrometer. Thus, $^1$H NMR gives no additional proof of the compound structure. The macroinitiator **8** was obtained by the reaction of precursor **7** with *N*-bromosuccinimide. The success of this reaction was confirmed by the peak from 4.2 to 4.5 ppm in the $^1$H NMR spectrum of the macroinitiator (Figure 10a). Integration of this peak vs the aromatic signals (6.0−7.1 ppm) indicated a degree of bromination of 51%, which was also confirmed by elemental analysis. Following the procedures used for unfunctionalized polymer brushes,[36] the macroinitiator **8** was used for the synthesis of end-functionalized polymer brushes from poly(styrenesulfonate dodecyl ester) (**9**). The $^1$H NMR spectrum of this substance (**9**) obtained is included in Figure 10a. The signal group from 6.0 to 8.0 ppm corresponds to the sum of all aromatic protons, the signal at 3.8 to 4.2 ppm originates from the α-$CH_2$ group from the $C_{12}H_{25}$ side chain. The absence of a peak from 4.2 to 4.5 ppm suggests that all initiating sites of the macroinitiator were consumed. Thus, an end-functionalized polymer brush with ∼50% branching density was obtained. The peak group from 0.5 to 2.5 ppm corresponds to the aliphatic backbone and the side chains. By the same method as outlined in reference 36, the side chain length was determined as $n_n = 9$ (minimum value, as 100% initiation efficiency was assumed). The solubility of the end-functionalized polymer brush **9** in THF and $CH_2Cl_2$, compared to an unfunctionalized PSSD polymer brush, was unexpectedly low. Rather than dissolving properly, the substance swelled with solvent, leaving a gel-like precipitate. It only dissolved completely after increasing the solvent amount by a factor of 20. This could be due to the loss of a few dodecyl ester groups during the reaction or during work up. The resulting negative charge finds the positive head group, forming a polyelectrolyte complex with low solubility. If the complexation was merely intramolecular, this would not have such a drastic effect on the solubility. Shielding of these electrostatic interactions by salt addition increases the solubility again. This complexation is an indication why nature, being an efficient designer, uses such a complicated linker to connect the anionic polyelectrolyte brushes with hyaluronic acid. In this claw-shaped linker molecule, the positive charges are pointing to the inside of the claw and are surrounded by a noncharged periphery. Thus, self-complexation or inter-brush complexation is avoided, as only a molecule fitting into the claw can form the complex. From this point of view, the aggregation between proteoglycans and hyaluronic acid is not only an example of ionic self-assembly, but also of the host−guest principle. The desired polyelectrolyte brush structure **10** was obtained by reaction of the poly(styrenesulfonate dodecyl ester) **9** with trimethylsilyl iodide, followed by base hydrolysis. The sample was analyzed by static and dynamic light scattering and cryo-TEM. The light scattering results are displayed in Figure 10b. $M_w$ was determined to be $1.9 \times 10^6$ g mol$^{-1}$. This value is on the same order of magnitude as the molecular weight of the proteoglycans in cartilage.[5] The radius of gyration $R_{g,z}$ was 68.1 nm, and $R_h$ was determined from dynamic light scattering as 46.8 nm, giving a ratio $\rho = R_{g,z}/R_h$ of 1.45. This is a reasonable value for polymer brushes with a certain degree of flexibility.[49] In the cryo-TEM images (Figure 11), long wormlike shapes are found. These have a diameter of $9 \pm 4$ nm, which is of the same order of magnitude as for the nonfunctionalized brushes discussed above. One striking feature of these brushes (Figure 11), as compared to these nonfunctionalized brushes (Figure 7a) is that they tend to attach end-on to all kinds of heterogeneities of the sample, from drop-like impurities of various diameters to the pore edges of the holey carbon films on the gold grid that hold the cryo-TEM sample. This is a strong indication that complex formation with this simple model compound with only two positive charges as a linker molecule is possible. To further test the ability of the above-described functionalized polyelectrolyte brushes to in-

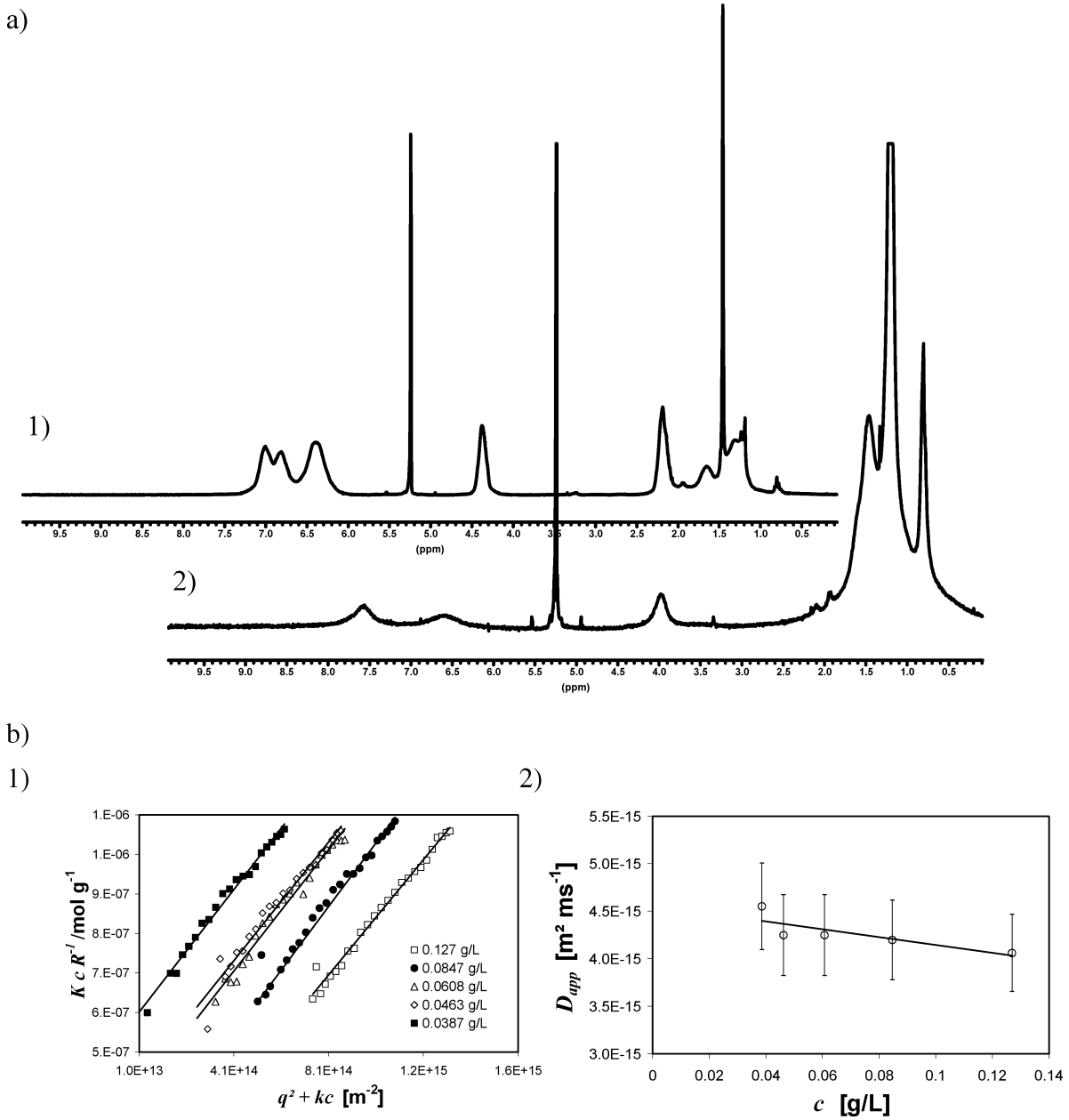


**Figure 10.** Characterization of the functionalized polyelectrolyte brushes. (a) $^1$H NMR spectra of macroinitiator **8** (1) and the polymer brush **9** (2) (both in $CD_2Cl_2$); (b) Light scattering results of polyelectrolyte brush **10**: (1) molecular mass determination by static light scattering (Zimm plot); (2) determination of the hydrodynamic radius by dynamic light scattering.

teract with negatively charge species, it was attempted to complexate the brushes to a spherical negatively charged latex particle. This geometry was chosen to simplify the interpretation of the analytical results. An aqueous solution of polyelectrolyte brush **10** ($c$ = 0.1 g L$^{-1}$, 3 mL, pH adjusted to 9 with 0.1 M NaOH) was mixed with a solution of a negatively charged spherical Latex particle (poly(styrene-acrylic acid) latex particle with 4% acrylic acid, negative surface charge due to $COO^-$ groups (cf. ref 53), $c_{latex}$ = 1 $\mu$L, $c$ = 0.1 g L$^{-1}$). First, the components (brush and latex) were characterized separately by dynamic light scattering. The results are given in Figure 12a. The hydrodynamic radius of the brush was determined as 46 nm with a relatively broad distribution, while the latex particle had an $R_h$ of 37 nm, with a sharper distribution. Directly after mixing, a broad peak corresponding to a particle with $R_h$ = 55.0 nm was found (see Figure 12a), while two diffusion processes corresponding to objects with $R_h$ = 52.8 nm and $R_h$ = 139 nm were found after 24 h (red squares in Figure 12a). As a control experiment, the same mixture was investigated at pH 2, where the carboxylic acid groups of the latex particle were not dissociated. Here, no aggregation was found. Similar experiments with nonfunctionalized polyelectrolyte brushes at pH 9 also did not lead to aggregate formation. These results lead to the following interpretation: As the measurement of the polyelectrolyte brushes in water indicates, these molecules are, at the given dilution conditions, not significantly self-aggregating. Directly after mixing, there is barely any interaction between latex and brush, as the value of $R_h$ measured for the individual particles is close to the $R_h$ value determined for the mixture. After 24 h, large aggregates are formed, which are almost out of the light scattering regime. The particle size roughly corresponds to the value expected for a central particle with 37 nm radius, surrounded by a layer of polyelectrolyte brushes with a hydrodynamic radius of 46 nm (Figure 12b). As an answer to the question why these functionalized brushes preferentially aggregate with the latex and not with themselves,

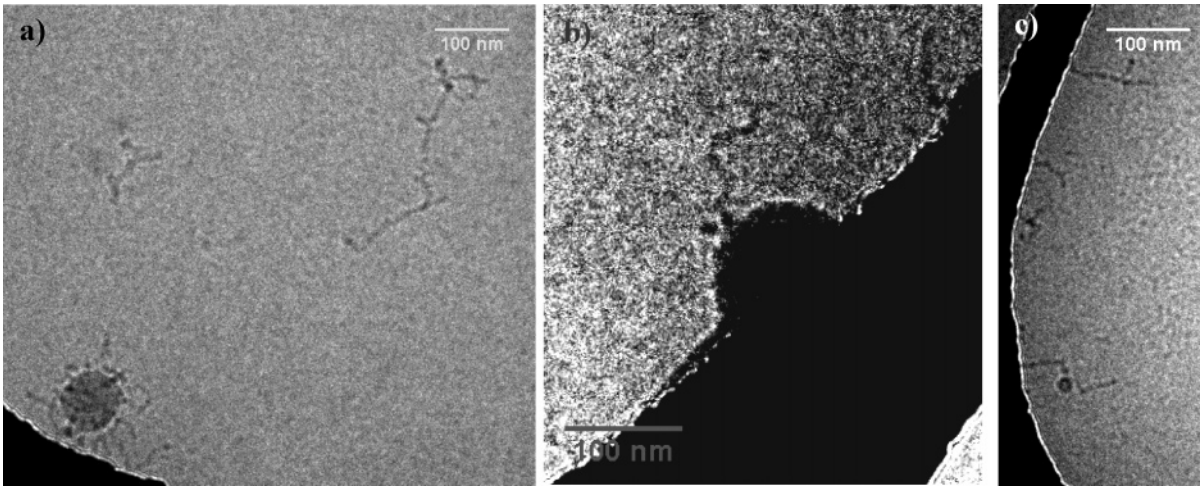


**Figure 11.** Characterization of the functionalized polyelectrolyte brushes: Cryo-TEM images of polyelectrolyte brush **10**. Parts a and b depict a sample inhomogeniety to which the polyelectrolyte brushes are attached end-on (b) also shows an agglomerate of uncomplexated polyelectrolyte brushes). Part c shows end-on attachment of the brushes onto the gold support grid.

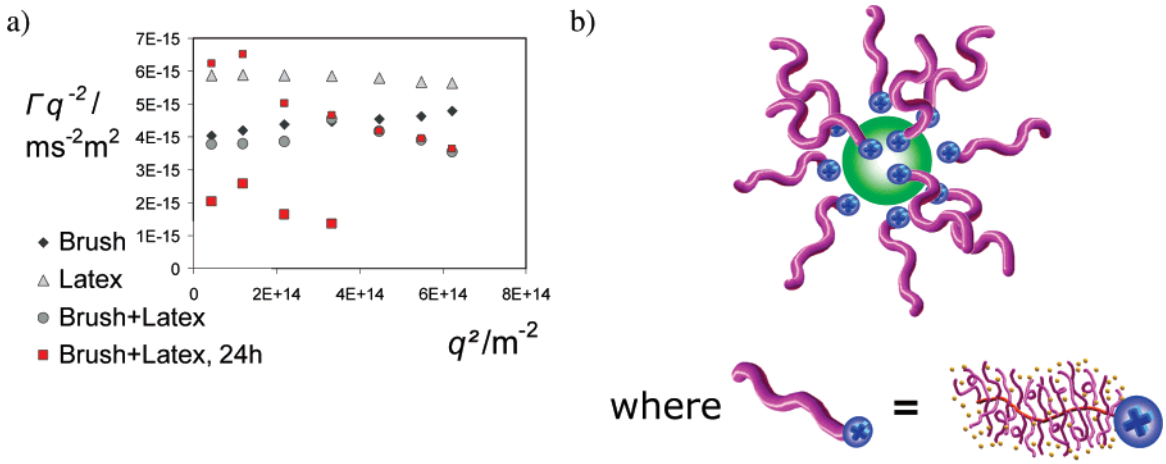


**Figure 12.** Complexation experiments monitored by dynamic light scattering. (a) A solution containing only the polyelectrolyte brush **10** (rhombs) or the latex (triangles) shows one diffusive process. Directly after mixing (circles), only one diffusive process is observed in a solution containing brush and latex. After 24 h, two diffusive processes are observed (red squares), which can be attributed to the formation of brush−latex aggregates. (b) Cartoon representation of the polyelectrolyte brush−latex complex.

the following is suggested: due to the counterion condensation, which is significantly higher for polyelectrolytes with brushlike architecture as compared to their linear analogues,[32] charges on the end group do not "see" the negative charges of the brushes, thus a complexation to the latex surface is preferred.

## Conclusion

On the pathway to polyelectrolyte brushes from poly(styrenesulfonate) as a synthetic model compound for the proteoglycans in cartilage, the following was achieved:

**1. Cylindrical polyelectrolyte brushes from styrenesulfonate without end-group** were synthesized from the corresponding dodecyl and ethyl esters. These brushes were characterized in solution and on solid interfaces. It was shown that these brushes may form huge aggregates in solution. With the concept of a hydrophobic gradient within the polyelectrolyte brushes, some of their solution and aggregation behavior can be understood. The fact whether a specific sample dissolves as a single molecule or as an aggregate depends on the degree of saponification, the grafting density and the side chain length, which both influence the $A_2$ value. Because of the limited sample matrix available, no firm conclusions can yet be drawn, however the following trends seem to be meaningful:

**(a) Samples with Identical Grafting Density, Backbone Length, and Side Chain Length.** The higher the degree of hydrolysis, the smaller the aggregates, as demonstrated for polyelectrolyte samples derived from the parent ester **3-30-D1** (Table 2b).

**(b) Samples with Identical Degree of Hydrolysis and Backbone Length, but Different Side Chain Lengths and Grafting Densities.** From the data on the parent ester[36] (which we consider to be more reliable than the data obtained on the polyelectrolyte in aqueous solution), it is shown that the side chain lengths of **11-40-VId** and **11-30-2d** are significantly longer (9 and 22, respectively) than for sample **11-60-Id** with on average 3 repeat units per side chain. The grafting densities increase in the order **11-30-2d** < **11-40-Id** < **11-60-Id**. Both samples **11-60-Id** and **11-30-2d** are molecular disperse; however **11-40-VId** is not, due to an intramolecular hydrophobic gradient in the molecule. We therefore believe that, *at a given degree of saponification*, sufficiently low grafting densities *or* sufficiently low side chain lengths are necessary to obtain molecularly disperse solutions. In between, there is a regime where aggregates form. Even sample **3-30-1d**, with a different backbone, fits into this picture: it has relatively long side chains ($n_n = 18$), but the grafting density is low enough to allow for molecularly disperse solution behavior.

**(c)** If aggregates form, the size and shape that the aggregates seem to have is influenced by the side chain-backbone length ratio: for longer backbones, larger and more complex aggregate shapes were observed, as shown for samples **11-40-IVd**.

For more quantitative statements, more samples would be necessary. The samples discussed here were obtained in the process of establishing and optimizing a complicated synthetic procedure with many reaction parameters. Thus, the products obtained, though being well-defined, do not feature the systematic variation of side chain length, backbone length and grafting density that might be wished for to obtain a more complete picture. Now that the synthesis of such molecules is established, and some striking and unexpected structural features were found, samples with systematically varied molecular parameters should be synthesized for a complete understanding of their influence of the molecular shape and aggregation behavior.

As it was not possible to obtain quantitatively saponified polyelectrolytes from the reactions described above, solvent free reactions such as pyrolysis may be considered as an alternative. As this is a solid-state reaction, the osmotic pressure does not have such a drastic effect on reaction conversion. It was shown by Corey[51] that for aromatic sulfonate esters with alkyl substitution in the para-position, the yield for this reaction is only 56% at 150 °C. At this temperature, the structural integrity of the polymer backbone might also suffer. However, a very recent paper[52] suggests that poly(styrenesulfonate neopentyl ester) may be thermolyzed quantitatively without loss of the structural integrity of the sample. Thus, switching to this monomer may solve the encountered difficulties. Some "side products" of this project might be of further interest: the extended and complicated aggregates of the unfunctionalized brushes may be used as templates for the production of nanowires. The gradient brushes, which have been shown to be able to solubilize a water-insoluble organic dye, may be used for delivery of such molecules into hydrophilic, water-containing compartments, i.e., in organisms, for drug delivery. It would be interesting to investigate whether it is possible to trigger the release of such molecules by external stimuli.

**2. Cylindrical polyelectrolyte brushes from styrenesulfonate with end-group** were synthesized using an ATRP macroinitiator with a positively charged head group. After careful characterization of the precursors and the polyelectrolyte brushes **10** in solution, complexation experiments with **10** and negatively charged latex particle were conducted. The end-functionalized polyelectrolyte brushes were found to form complexes with negatively charged latex particles. It has thereby been demonstrated that our simplified model polyelectrolyte brushes are able to mimic the proteoglycan molecules and thus are a suitable components for a "first approximation" model of the proteoglycan−hyaluronic acid aggregate. Care must be taken that the degree of saponification of the brushes is high and that the side chains are short enough to avoid the building-up of a gradient in the molecule after saponification, as this leads to aggregation due to hydrophobic interactions as shown in the first section of this paper. The functionalized *polymer* brushes **9** were strongly self-aggregating on the pre-polyelectrolyte level due to loss of a few ester groups, forming a solvent-swollen gel. Although this was a major drawback for the formation of well-defined "brush of brushes" -like aggregates with the polymer brushes **9**, it shows that we are on the right track—this gel-like material, while having only a slightly different chemical structure as compared to the unfunctionalized brushes, shows entirely different mechanical and solution properties. The functionalized *polyelectrolyte* brushes **10** have the desired property of attaching to negatively charged entities. All that is left to do is to direct this aggregation tendency toward more organized structures and characterize the resulting materials. For possible applications as cartilage substitutes, care should be taken at a more advanced stage of the project that all materials used are biocompatible and nonbiodegradable.

For further synthetic attempts to model the proteoglycan−hyaluronic acid complex, the following strategies are currently investigated: With the present system, complexation experiments with linear, negatively charged poly(para-phenylene micelles) will be conducted to further prove the ability of these molecules to attach to negatively charged entities. With this model complex, rheological investigations could be carried out to examine the difference of the mechanical properties of simple brushes and the model complex.

**Acknowledgment.** We thank C. Rosenauer for measuring the refractive index increments; K. Kirchhoff for the TEM measurements, K. Klein for SANS measurements, P. Kindervater for the NMR measurements, and S. Türk and Ali Rohanipour for MALDI−TOF measurements. The latex was generously supplied by Dr. Rafael Muñoz-Espí, MPI−P Mainz. We further thank Prof. M. Schmidt, University of Mainz, for his critical comments and suggestions on the sample characterization. Financing from Max-Planck Society and Fonds der Chemischen Industrie is gratefully acknowledged.

## References and Notes

(1) Lehninger, A. L.; Nelson, D.; Cox, M. M. *Principles of Biochemistry*; Worth Publishers: New York 1993.
(2) Day, A. J.; Prestwich, G. D. *J. Biol. Chem.* **2002**, *277* (7), 4585.
(3) Alberts, B. *Molecular Biology of the Cell*; Francis & Taylor: New York 2002.
(4) Toole, B. P. *J. Clin. Invest.* **2000**, *106*, 335.
(5) Knudson, C. B.; Knudson, W. *Semin. Cell. Dev. Biol.* **2001**, *12*, 69.
(6) Kahmann, J. D.; O'Brien, R.; Werner, J. M.; Heinegård, D.; Ladbury, J. E.; Campbell, I. D.; Day, A. J. *Structure* **2000**, *8*, 763.
(7) Blundell, C. D.; Kahmann, J. D.; Perczel, A.; Mahoney, D. J.; Cordell, M. R.; Teriete, P.; Campbell, I. D.; Day, J. A. Getting to grips with HA-protein interactions. In *Hyaluronan 2000*; Kennedy, J. F., Ed.; Woodhead Publishing Ltd.: Cambridge, U.K., 2001.
(8) Wintermantel, M.; Gerle, M.; Fischer, K.; Schmidt, M.; Wataoka, I.; Urakawa, H.; Kajiwara, K.; Tsukahara, Y. *Macromolecules* **1996**, *29*, 978.
(9) Fischer, K.; Schmidt, M. *Macromol. Rapid Commun.* **2001**, *22*, 787.
(10) Zhang, B. Dissertation, Universität Mainz 2004.
(11) Wahnes, C. Dissertation, Universität Mainz 2005.
(12) Fischer, K.; Gerle, M.; Schmidt, M. *Proc. ACS, PMSE Anaheim* **1999**, *30*, 133.
(13) Tsukahara, Y.; Inoue, J.; Ohta, Y.; Kohiya, S. *Polymer* **1994**, *35*, 5785.
(14) Sheiko, S. S.; Gerle, M.; Möller, M. *Langmuir* **1997**, *13*, 5368.
(15) Namba, S.; Tsukahara, Y.; Kaeriyama, K.; Okamoto, K.; Takahashi, M. *Polymer* **2000**, *41*, 5165.
(16) Deffieux, A.; Schappacher, M. *Macromolecules* **1999**, *32*, 1797.
(17) Schappacher, M.; Billaud, C.; Paulo, C.; Deffieux, A. *Macromol. Chem. Phys.* **1999**, *200*, 1377.
(18) Schappacher, M.; Bernard, J.; Deffieux, A. *Macrom. Chem. Phys.* **2003**, *204*, 762.
(19) Radke, W.; Müller, A. H. E. *Macromolecules* **2005**, *38*, 3949.
(20) Beers, K. L.; Gaynor, S. G.; Matyjaszewski, K.; Sheiko, S. S.; Möller, M. *Macromolecules* **1998**, *31*, 9413.
(21) Börner, H. G.; Beers, K. L.; Matyjaszewski, K.; Sheiko, S. S.; Möller, M. *Macromolecules* **2001**, *34*, 4375.
(22) Cheng. G.; Böker, A.; Zhang. M.; Krausch, G.; Müller, A. H. E. *Macromolecules* **2001**, *34*, 6683.
(23) Zhang, M.; Breitner, T.; Mori, H.; Müller, A. H. E. *Polymer* **2003**, *44*, 1449.
(24) Zhang, B.; Fischer, K.; Schmidt, M. *Macromol. Chem. Phys.* **2005**, *206*, 157.
(25) Muthukrishnan, S.; Zhang, M.; Burkhardt, M.; Drechsler, M.; Mori, H.; Müller, A. H. E. *Macromolecules* **2005**, *38*, 7926.

(26) Tsukahara, Y.; Mizuno, K.; Segawa, A.; Yamashita, Y. *Macromolecules* **1989**, *22*, 1546.
(27) Tsukahara, Y.; Tsutsumi, K.; Yamashita, Y.; Shimada, S. *Macromolecules* **1990**, *23*, 5201.
(28) Wintermantel, M.; Gerle, M.; Fischer, K.; Schmidt, M.; Wataoka, I.; Urakawa, H.; Kajiwara, K.; Tsukahara, Y. *Macromolecules* **1996**, *29*, 978.
(29) Wintermantel, M.; Schmidt, M.; Tsukahara, Y.; Kajiwara, K.; Kohjiya, S. *Macromol. Rapid Commun.* **1994**, *15*, 279.
(30) Dziezko, P.; Sheiko, S. S.; Fischer, K.; Schmidt, M.; Möller, M. *Angew. Chem., Int. Ed.* **1997**, *36*, 2812.
(31) Gerle, M.; Fischer, K.; Roos, S.; Müller, A. H. E.; Schmidt, M.; Sheiko, S. S.; Prokhorova, S.; Möller, M. *Macromolecules* **1999**, *32*, 2629.
(32) Rühe, J.; Ballauf, M.; Biesalski, M.; Dziezok, P.; Gröhn, F.; Johannsmann, D.; Houbenov, N.; Hugenberg, N.; Konradi, R.; Minko, S.; Motornov, M.; Netz, R. R.; Schmidt, M.; Seidel, C.; Stamm, M.; Stephan, T.; Usov, D.; Zhang, H. *Adv. Polym. Sci.* **2004**, *165*, 79.
(33) Fernyhough, C. M.; Young, R. N.; Ryan, A. J.; Hutchings, L. R. *Polymer* **2006**, *47*, 3455.
(34) Papagiannopoulos, A.; Fernyhough, C. M.; Waigh, T. A. *J. Chem. Phys.* **2005**, *123*, 214904.
(35) Papagiannopoulos, A.; Waigh, T. A.; Fluerasu, A.; Fernyhough, C. M.; Madsen, A. *J. Phys.: Condens. Matter* **2005**, *17*, 279.
(36) Lienkamp, K.; Ruthard, C.; Lieser, G.; Berger, R.; Gröhn, F.; Wegner, G. *Macromol. Chem. Phys.* **2006**, *207*, 2050.
(37) Woeste, G.; Meyer, W.; Wegner, G. *Makromol. Chem.* **1993**, *194*, 1237.
(38) Wittig, G.; Schöllkopf, U. *Chem. Ber.* **1954**, *87*, 1318.
(39) Quirk, R. *Br. Polym. J.* **1990**, *23*, 47.
(40) Becker, A.; Köhler, W.; Müller, B. *Ber. Bunsen-Ges. Phys. Chem.* **1995**, *99*, 600.
(41) Okamura, H.; Takatori, Y.; Tsunooka, M.; Shirai, M. *Polymer* **2002**, *43*, 3155.
(42) (a) Provencher, S. W. *Comput. Phys. Commun.* **1982**, *27*, 213. (b) Provencher, S. W. *Comput. Phys. Commun.* **1982**, *27*, 229.
(43) Kratchovil, P. *Classical light scattering from polymer solutions*; Elsevier: Amsterdam, 1987; p 145.
(44) Burchard, W. Combined Static and Dynamic Light Scattering. In *Light Scattering, Principles and Development*; Brown, W., Ed.; Claredon Press: Oxford, U.K., 1996.
(45) Schmidt, M. *Combined Static and Dynamic Light Scattering*", in: *Dynamic Light Scattering*; Brown, W., Ed.; Claredon Press: Oxford, U.K., 1993.
(46) Wittemann, A.; Drechsler, M.; Talmon, Y.; Ballauff, M. *J. Am. Chem. Soc.* **2005**, *127*, 9688.
(47) Matsumoto, K.; Hasegawa, H.; Matsuoka, H.; Hideki, M. *Tetrahedron* **2004**, *60*, 7197.
(48) Lienkamp, K. Dissertation, Universität Mainz, 2006.
(49) Green, F. *The Sigma-Aldrich Handbook of stains, dyes & indicatiors*, Aldrich Chemical Company: Milwaukee, WI, 1991; p 263.
(50) Wahnes, C. Dissertation, Universität Mainz, 2005.
(51) Corey, E. J.; Posner, G. H.; Atkinson, R. F.; Wingard, A. K.; Halloran, D. J.; Radzik, D. M.; Nash, J. J. *J. Org. Chem.* **1989**, *54*, 389.
(52) Baek, K. Y.; Balsara, N. P. *PMSE Prepr.* **2005**, *92*, 7.
(53) Muñoz-Espí, R. Dissertation, Universität Mainz, 2006.

MA062569B